Chemical Geology 357 (2013) 52–66

Contents lists available at ScienceDirect

Chemical Geology

journal homepage: www.elsevier.com/locate/chemgeo

Research paper

Source of highly potassic basalts in northeast China: Evidence from Re–Os, Sr–Nd–Hf isotopes and PGE geochemistry

Zhu-Yin Chu [a,*], Jason Harvey [b], Chuan-Zhou Liu [a], Jing-Hui Guo [a], Fu-Yuan Wu [a], Wei Tian [c], Yan-Long Zhang [d], Yue-Heng Yang [a]

[a] State Key Laboratory of Lithospheric Evolution, Institute of Geology and Geophysics, Chinese Academy of Sciences, Beijing 100029, China
[b] School of Earth and Environment, University of Leeds, Leeds LS2 9JT, UK
[c] Key Laboratory of Orogenic Belts and Crustal Evolution, MOE, School of Earth and Space Sciences, Peking University, Beijing 100871, China
[d] College of Earth Sciences, Jilin University, Changchun 130026, China

ARTICLE INFO

Article history:
Received 23 August 2012
Received in revised form 1 August 2013
Accepted 6 August 2013
Available online 17 August 2013

Editor: L. Reisberg

Keywords:
Re–Os isotopes
PGE
Sulphide
Sr–Nd–Hf isotopes
Potassic basalts
NE China

ABSTRACT

The origin of the very young (0.5 Ma to 1721 AD) Wudalianchi-Erkeshan (WDLC and EKS) highly potassic basalts in northeast (NE) China has been the subject of considerable debate. In this study, we present new major-, trace- and platinum group element (PGE) data together with Re–Os, Lu–Hf, and Sr–Nd isotopic analyses for these potassic basalts in order to further constrain their source. It has been shown that the WDLC and EKS basalts have unradiogenic to only moderately radiogenic osmium isotope ratios with $^{187}Os/^{188}Os$ ranging from 0.1187 to ~0.17, and only slight PPGE (Pt and Pd) enrichments relative to IPGE (Os, Ir and Ru). The positive correlations between $^{187}Os/^{188}Os$ and 1/Os suggests that these basalts have probably experienced about 2–8% of lower continental crust addition during magma ascent. On the other hand, the incorporation of sub-continental lithospheric mantle (SCLM)-derived, primary sulphides and/or PGE micro-alloys during magma ascent seems likely in some basalts, which preserve particularly unradiogenic Os compositions. The complex interplay of signatures derived from crustal and SCLM contamination means that the Os isotope systematics of the basalts do not unequivocally fingerprint the source of the WDLC and EKS basalts.

The strong enrichments of light rare earth elements (LREE) and large ion lithophile elements (LILE), high-K, EM1-like Sr–Nd–Hf isotopic characteristics, and particularly strong fractionation of the heavy REE ($(Sm/Yb)_N = 9.7 \pm 0.6$), suggest that the WDLC and EKS basalts mainly originated from phlogopite-bearing garnet-peridotite in the SCLM. Combined with low Ce/Pb ratios (~9.4–13.5), the most likely source of WDLC and EKS basalts is SCLM that has been metasomatized by delaminated old, lower continental crust. This is different from previous hypotheses that implicate a dominantly asthenospheric source with a contribution from delaminated ancient SCLM or subducted oceanic crust with sediments, or a SCLM source that has been metasomatized by melts derived from deep asthenosphere during the Proterozoic.

1. Introduction

Cenozoic volcanic rocks, predominantly alkaline basalts, are widely distributed in Northeastern China (NE China) (Fig. 1), and form an important part of the West Pacific volcanic zone (e.g., Zhang et al., 1991, 1995, 1998, 2000; Zou et al., 2000; Liu et al., 2001; Zou et al., 2003; Choi et al., 2006; Chen et al., 2007; Yan and Zhao, 2008). However, their petrogenesis remains equivocal, despite numerous detailed prior investigations of the area. Interpreting the significance of the composition of Cenozoic alkaline basalts from NE China is further complicated by the complex and varying structure for the mantle beneath this region, as suggested by earlier studies (e.g., Zhang et al., 2000; Zou et al., 2000, 2003; Choi et al., 2006; Chen et al., 2007; Yan and Zhao, 2008; Zhang et al., 2011).

Among the Cenozoic basalts in NE China, the three potassic volcanic areas of Wudalianchi (WDLC), Erkeshan (EKS) and Keluo (KL), together comprise the Wudalianchi–Erkeshan–Keluo (WEK) volcanic field. This field is located in the Xing'an Mongolian Orogenic Belt (XMOB) at the boundary between the northwestern margin of the Songliao Basin and the Great Xing'an Ranges, in the western Heilongjiang Province, NE China (Fig. 1). The geochemical features of the WDLC, EKS and KL basalts (e.g., Zhang et al., 1991, 1995, 1998; Zou et al., 2003) are similar to those of EM1-derived basalts (Zindler and Hart, 1986) and dramatically different from those of Cenozoic basalts found elsewhere in eastern China (e.g., Zhou and Armstrong, 1982; Peng et al., 1986; Song et al., 1990; Zhi et al., 1990; Basu et al., 1991; Fan and Hooper, 1991; Liu et al., 1994; Chen et al., 2007).

Although the peculiar composition of the WEK potassic basalts in NE China has been well documented, the origin of intraplate volcanism in this region is still the subject of debate, resulting in several competing theories as to their origin: (i) Based upon their Sr–Nd–Pb isotopic and

* Corresponding author. Tel.: +86 10 82998586; fax: +86 10 62010846.
E-mail address: zhychu@mail.igcas.ac.cn (Z.-Y. Chu).

0009-2541/$ – see front matter © 2013 Elsevier B.V. All rights reserved.
http://dx.doi.org/10.1016/j.chemgeo.2013.08.007

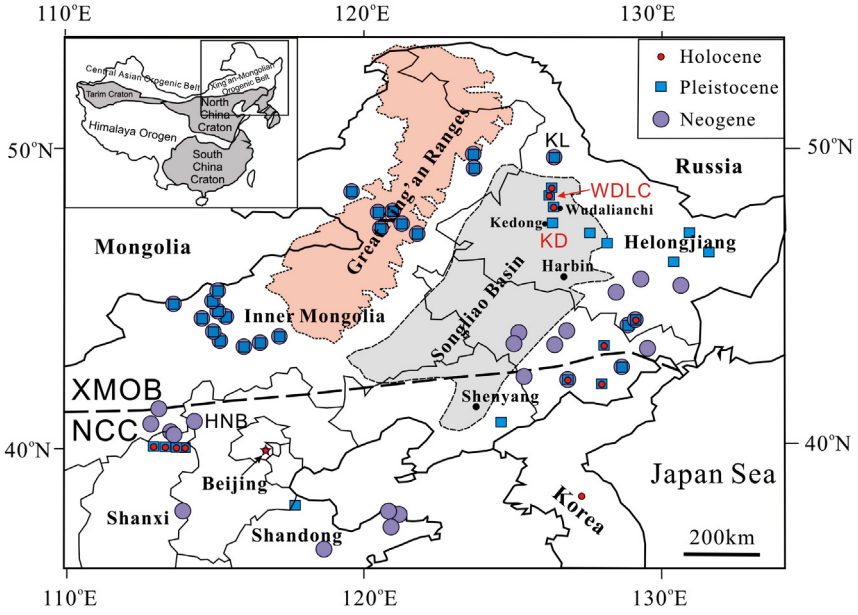

Fig. 1. Sketch map of Northeast (NE) China (modified after Chen et al., 2007), in which the Cenozoic basalts, Great Xing'an Ranges, Songliao Basin and the locations of the Wudalianchi, Erkeshan and Keluo volcanic rocks are shown. Dashed line is the approximate boundary between the North China Craton (NCC) and Xing'an Mongolian Orogenic Belt (XMOB); Abbreviations of volcanic fields are as follows: WDLC (Wudalianchi), KD (Kedong), KL (Keluo) and HNB (Hannuoba).

trace elemental fingerprint, which resembles an EM1 mantle component, it has been suggested that the WEK potassic basalts were produced by small-degree (5–7%) melting of ancient SCLM, which has subsequently been overprinted by Proterozoic metasomatism after its formation (Zhang et al., 1995, 1998, 2000). A phlogopite-bearing garnet peridotite source within the 120 km thick lithosphere at this locality has been suggested as a probable source (Zou et al., 2003); (ii) Based upon the similarities in incompatible trace element concentrations with OIB, Choi et al. (2006) argued that the WEK basalts originated in the shallow asthenosphere which contains fragments of delaminated SCLM from the eastern North China Craton (NCC). The likely presence of "plum-pudding" mantle (e.g., Phipps Morgan and Morgan, 1999) beneath NE China (Flower et al., 1998) and basaltic Sr–Nd–Pb–Hf isotopic characteristics resembling a DMM-EM1 array have been cited as strong evidence against a SCLM origin for the WEK basalts (Choi et al., 2006); (iii) Mixing FOZO (Focal Zone; Hart et al., 1992) and LoMu (low U/Pb; Douglass et al., 1999) mantle sources, instead of an EM1-like SCLM mantle source, has been advocated by Chen et al. (2007); (iv) More recently, Kuritani et al. (2013) argued that the WDLC and EKS basalts originated from a mantle transition zone which has been metasomatized by K-rich sediment-derived fluids ~1.5 Ga ago, through the stagnation of an ancient slab.

In addition, although wholesale contamination of the WDLC and EKS basalts by the upper crust can largely be discounted, based on trace elemental and Sr–Nd–Pb isotopic results (Zhang et al., 1995, 1998; Zou et al., 2003), previous studies have not been able to unequivocally exclude the possible influence of less evolved lower crust in the petrogenesis of the WDLC and EKS basalts (Zhang et al., 1995, 1998; Zou et al., 2003). Unlike the lithophile-element based Sr–Nd–Pb isotope systems, Os isotopes can be particularly sensitive to crustal contamination which generates isotope ratios that are distinct from those of mantle sources (e.g., Chesley and Ruiz, 1998; McBride et al., 2001; Chesley et al., 2004; Jung et al., 2011). Basaltic melt, contaminated during its ascent through old continental crust, should develop a radiogenic Os isotopic signature. In contrast, basalts originated from an enriched old lithospheric mantle source would retain unradiogenic to only moderately radiogenic Os isotopic compositions (e.g., McBride et al., 2001; Chesley et al., 2004; Rudnick and Walker, 2009). Therefore, Re–Os isotopes, together with PGE elemental abundances can provide important constraints on the relative involvement of crustal materials in the petrogenesis of the very young WDLC and EKS basalts.

Accordingly, this study presents new major-, trace- and platinum group element (PGE) abundances together with Os, Hf and Sr–Nd isotopic data, for the WDLC and EKS potassic basalts to further constrain their origin and the nature of the underlying SCLM. Since the nearby Keluo basalts contain abundant mantle xenocrysts, they have not been investigated for Re–Os isotopes and PGE geochemistry here. Based upon new analyses, it seems likely that the WDLC and EKS basalts were mainly generated in SCLM which has been metasomatized by recycled old lower continental crust materials. Although crustal contamination during magma ascent has not materially affected the elemental abundances of incompatible, lithophile elements and the Sr–Nd–Hf isotope systems, evidence for low degrees of lower crustal contamination is preserved in some basalts with particularly low Os abundances.

2. Geological background and sample descriptions

The XMOB, part of the Central Asian Orogenic Belt (CAOB), is a composite fold belt more than 1500 km wide, formed during a long period (Paleozoic to early Mesozoic) of subduction and collision between the Siberian Craton in the north and the NCC in the south (Sengör et al., 1993). The potassic basalts of the WEK field, located in XMOB (Fig. 1), are distributed over an area of >1400 km^2. Among them, the WDLC and EKS potassic basalts were erupted from about 0.5 Ma ago onwards (Zhang et al., 1995; Liu et al., 2001). Two of the Wudalianchi cones, Laoheishan and Huoshaoshan, erupted during 1719–1721 AD, according to the Qing Dynasty Records (Zou et al., 2003). The potassic rocks consist mainly of olivine leucitite and leucite basanite.

The samples studied here were collected from lava flows related to the eruptions of Laoheishan (LHS) (1721 AD), Huoshaoshan (HSS) (1721 AD) and Yaoquanshan (YQ) (0.25 Ma, Zhang et al., 1995) from the Wudalianchi volcanic area, and lava flows related to the Erkeshan eruption (0.56 Ma, Liu et al., 2001) from the Kedong (KD) volcanic area (Fig. 1). The sample locations (latitude and longitude) are listed in Table 1. The detailed descriptions of the samples and petrography of some representative samples are shown in the electronic supplement (Appendix 1).

Table 1
Elemental compositions of the WDLC and EKS basalts.

Sample	YQ1	YQ3	YQ4	YQ6	YQ7	YQ8	LHS1	LHS3	LHS4	LHS6	HSS2	HSS5
Location	48′39.020″N, 126′09.333″E			48′39.326″N, 126′08.973″E			48′42.456″N, 126′07.110″E			48′43.061″N, 126′07.645″E	48′44.230″N, 126′10.257″E	
Major element (wt.%)												
SiO_2	52.74	53.06	49.71	52.99	49.67	49.21	51.63	51.73	51.87	53.24	53.21	53.54
TiO_2	2.45	2.45	2.39	2.72	2.35	2.34	2.30	2.29	2.77	2.34	2.42	2.42
Al_2O_3	13.88	13.88	12.15	14.39	13.42	13.25	13.49	13.53	13.68	13.99	13.94	14.02
TFe_2O_3[b]	8.49	8.48	9.20	8.37	9.55	9.64	8.89	8.93	8.89	8.19	8.24	8.27
MnO	0.11	0.11	0.12	0.10	0.13	0.13	0.12	0.12	0.11	0.11	0.11	0.10
MgO	6.17	6.18	9.47	4.45	7.40	7.69	7.45	7.46	6.21	5.96	5.93	5.99
CaO	5.50	5.46	6.89	5.22	7.16	7.29	6.02	6.03	5.66	5.09	5.15	5.17
Na_2O	3.86	3.86	3.85	4.31	4.17	4.23	3.95	3.96	3.52	3.98	3.86	3.85
K_2O	5.53	5.53	4.50	6.09	4.83	4.73	4.95	4.95	5.87	5.53	5.63	5.64
P_2O_5	1.00	0.99	1.08	1.10	1.03	1.02	0.92	0.92	1.07	0.98	1.01	1.00
LOI	−0.04	−0.10	−0.02	−0.14	−0.14	−0.08	−0.18	−0.14	0.10	−0.02	−0.10	0.00
TOTAL	99.69	99.89	99.33	99.61	99.57	99.45	99.55	99.78	99.75	99.39	99.40	100.0
K_2O/Na_2O	1.43	1.43	1.17	1.41	1.16	1.12	1.25	1.25	1.67	1.39	1.46	1.46
Mg#	62.9	62.9	70.6	55.3	64.4	65.0	66.1	66.1	61.9	62.9	62.6	62.8
Trace element (ppm)												
Sc	11.7	12.3	12.1	12.2	12.2	11.7	12.2	12.1	13.8	14.4	14.5	14.1
Cr	190	194	193	187	185	186	182	181	171	265	195	218
Ni	158	161	161	159	157	155	156	156	134	207	151	164
Cu	31.8	33.3	32.1	32.5	32.3	31.9	33.2	33.0	30.4	38.1	35.2	32.3
Zn	114	118	116	116	115	109	116	114	112	122	119	120
Rb	107	111	110	111	110	110	114	112	116	92.3	100	96.6
Sr	1428	1486	1454	1470	1457	1456	1478	1447	1458	1752	1601	1641
Y	21.8	22.5	22.1	22.2	22.1	22.0	22.1	21.7	22.2	26.7	24.2	24.4
Zr	524	533	530	533	529	529	521	511	518	391	389	382
Nb	66.6	69.0	68.0	68.1	68.1	68.0	67.3	66.0	68.9	72.0	70.6	71.5
Ba	1575	1628	1586	1616	1607	1613	1702	1675	1893	1835	1822	1842
La	84.5	87.5	85.7	86.3	85.8	86.4	85.9	84.5	84.0	104	91.6	93.1
Ce	160	166	162	163	163	162	163	161	160	193	171	174
Pr	18.5	19.1	18.7	18.8	18.7	18.7	18.9	18.4	18.5	22.3	19.8	20.1
Nd	67.7	70.0	68.6	69.3	69.2	69.3	69.8	68.6	68.0	83.2	74.0	75.1
Sm	11.2	11.6	11.3	11.5	11.5	11.4	11.6	11.4	11.2	13.9	12.5	12.8
Eu	3.18	3.28	3.21	3.23	3.21	3.22	3.27	3.21	3.19	3.98	3.66	3.71
Gd	8.87	9.14	8.86	8.93	8.92	8.91	9.05	8.77	8.82	11.1	10.0	10.3
Tb	1.01	1.03	1.01	1.02	1.03	1.02	1.03	1.00	0.99	1.25	1.15	1.17
Dy	5.14	5.28	5.22	5.24	5.17	5.19	5.22	5.06	5.08	6.35	5.74	5.88
Ho	0.818	0.843	0.831	0.828	0.831	0.829	0.829	0.815	0.817	1.001	0.913	0.926
Er	1.97	2.03	1.99	1.97	1.97	1.96	1.98	1.92	1.95	2.33	2.12	2.14
Tm	0.232	0.244	0.236	0.237	0.236	0.240	0.236	0.228	0.231	0.269	0.248	0.250
Yb	1.31	1.34	1.31	1.31	1.32	1.33	1.29	1.29	1.30	1.46	1.34	1.34
Lu	0.174	0.180	0.174	0.175	0.171	0.179	0.173	0.171	0.176	0.198	0.180	0.179
Hf	11.6	11.8	11.7	11.8	11.6	11.7	11.6	11.3	11.4	8.5	8.5	8.40
Ta	3.57	3.60	3.58	3.67	3.74	3.83	3.88	3.99	3.81	3.87	3.99	4.07
Pb	16.4	17.5	16.5	16.4	16.2	16.6	16.1	15.8	16.2	14.3	13.6	13.8
Th	7.45	7.64	7.47	7.42	7.37	7.31	6.97	6.82	6.10	9.26	8.77	8.93
U	1.63	1.67	1.65	1.61	1.59	1.60	1.55	1.50	1.34	1.85	1.78	1.79
S	60	50	<50	50	<50	70	50	50	60	140	70	80
Element ratios												
Ce/Pb	9.8	9.5	9.8	9.9	10.0	9.7	10.1	10.2	9.9	13.5	12.6	12.6
La/Nb	1.27	1.27	1.26	1.27	1.26	1.27	1.28	1.28	1.22	1.45	1.30	1.30
Ba/Nb	23.7	23.6	23.3	23.7	23.6	23.7	25.3	25.4	27.5	25.5	25.8	25.8

[a] Reported values for the reference materials are from GeoREM (http://georem.mpch-mainz.gwdg.de/).
[b] Total Iron as Fe_2O_3; Mg# = $Mg^{2+}/(Mg^{2+} + Fe^{2+})$, assuming $Fe^{3+}/(Fe^{2+} + Fe^{3+}) = 0.15$.

3. Analytical methods

The rock samples were first sawn into chips, and surface contamination was completely removed during this step. The samples were then further split into small chips using a hammer wrapped in soft cloth. Small chips devoid of surface alteration and mantle or/and crustal xenocrysts, were chosen and cleaned with 10% hydrochloric acid in an ultrasonic bath for about half an hour. After ultrasonification, the chips were cleaned three times with deionized water. Subsequently, selected rock chips were crushed using an alumina ceramic jaw crusher, and then were ground into a fine powder in agate shatter-boxes. This produced 20–30 g of powder for each sample.

3.1. Elemental analysis

Major element data for whole-rock samples were obtained by X-ray fluorescence spectrometry (XRF) on fused glass disks using an Axios-Minerals instrument at the Institute of Geology and Geophysics, Chinese Academy of Sciences (IGGCAS), following the procedures of Chu et al. (2009). Precision is 1–3% RSD for elements

HSS6	HSS8	KD1	KD3	KD4	KD5	GSR-3 measured	GSR-3[a] reported	BCR-2 measured	BCR-2[a] reported	BHVO-2 measured	BHVO-2[a] reported
48′44.665″N 126′11.056″E		48′03.261″N, 126′13.919″E									
Major element (wt.%)											
49.02	53.51	52.37	52.68	52.48	52.32	44.58	44.64				
2.26	2.32	2.57	2.60	2.61	2.59	2.35	2.36				
12.98	13.95	13.62	13.57	13.51	13.56	13.78	13.83				
9.64	8.23	8.47	8.56	8.54	8.58	13.39	13.4				
0.14	0.11	0.11	0.11	0.11	0.11	0.17	0.17				
8.10	6.01	6.87	6.88	6.83	6.90	7.72	7.77				
7.44	5.14	5.42	5.34	5.35	5.36	8.78	8.81				
4.21	3.96	3.61	3.58	3.49	3.56	3.23	3.38				
4.58	5.48	5.66	5.74	5.73	5.65	2.31	2.32				
1.14	0.97	1.01	0.94	0.93	0.96	0.96	0.95				
−0.16	−0.24	−0.04	−0.24	−0.14	−0.08	2.28	2.24				
99.35	99.44	99.67	99.76	99.44	99.51	99.55					
1.09	1.38	1.57	1.60	1.64	1.59						
66.2	63.0	65.4	65.2	65.1	65.2						
Trace element (ppm)											
12.9	13.4	13.2	13.0	13.1	13.1			35.3	33	33.3	32
241	242	210	214	211	209			16.7	18	307	280
185	185	161	162	161	163			12.1	18	121	119
35.1	36.6	41.0	38.2	36.0	39.1			21.7	21	135	127
111	111	105	108	108	107			145	127	112	103
101	101	111	109	110	108			49.8	46.9	9.68	9.11
1330	1336	1537	1583	1574	1571			352	340	410	396
21.1	21.3	21.0	19.8	19.7	20.0			33.6	37	24.3	26
415	418	491	496	495	491			195	184	178	172
64.3	64.3	65.6	66.6	66.7	66.6			12.9	12.6	19.2	18.1
1591	1596	1915	1941	1936	1941			678	677	132	131
75.5	76.1	84.8	78.8	78.2	80.0			25.7	24.9	15.7	15.2
143	144	160	148	148	152			55.8	52.9	39.7	37.5
16.5	16.7	18.4	17.2	17.2	17.6			6.92	6.7	5.45	5.35
61.7	62.7	67.6	63.2	63.3	64.5			29.5	28.7	25.3	24.5
10.6	10.7	11.1	10.2	10.3	10.5			6.72	6.58	6.25	6.07
3.05	3.08	3.21	3.10	3.11	3.12			2.03	1.96	2.14	2.07
8.43	8.56	8.64	8.11	8.14	8.27			7.08	6.75	6.53	6.24
0.98	0.99	0.97	0.906	0.911	0.93			1.11	1.07	1.00	0.92
4.96	4.98	4.85	4.57	4.58	4.65			6.58	6.41	5.46	5.31
0.801	0.812	0.783	0.741	0.746	0.759			1.36	1.28	1.03	0.98
1.89	1.90	1.89	1.77	1.77	1.82			3.78	3.66	2.61	2.54
0.225	0.224	0.227	0.213	0.217	0.217			0.528	0.54	0.335	0.33
1.24	1.28	1.29	1.22	1.25	1.26			3.45	3.38	2.06	2
0.170	0.172	0.176	0.164	0.169	0.170			0.521	0.503	0.288	0.274
9.2	9.4	10.8	10.7	10.9	10.9			5.48	4.9	4.96	4.36
3.95	4.03	3.80	3.85	3.95	3.97			1.03	0.74	1.56	1.4
13.5	13.9	15.1	15.1	15.6	15.0			10.2	11	1.45	1.6
7.37	7.44	6.35	6.23	6.23	6.14			6.17	5.7	1.29	1.22
1.59	1.58	1.27	1.28	1.23	1.33			1.77	1.69	0.447	0.403
90	70	70	70	50	80			–		–	
Element ratios											
10.6	10.4	10.6	9.8	9.4	10.1						
1.17	1.18	1.29	1.18	1.17	1.20						
24.7	24.8	29.2	29.1	29.0	29.2						

present at >1 wt.%, and about 10% RSD for elements present at <1 wt.%. A Chinese basalt reference material, GSR-3, was analyzed during the same period, and the values determined are well within the range of consensus values (GeoREM, http://georem.mpch-mainz.gwdg.de/) (Table 1).

Trace element concentrations, including the rare earth elements (REE), were determined by inductively coupled plasma mass spectrometry (ICP-MS) using an Agilent 7500a system at IGGCAS, following the procedures described in Chu et al. (2009). Basalt reference materials BHVO-2 and BCR-2 were measured to monitor the accuracy of the analytical procedure, and the results are in good agreement with reference values (GeoREM, http://georem.mpch-mainz.gwdg.de/) (Table 1). Precision is generally better than 3% for most elements based on replicate analyses of several samples.

Sulfur concentrations were determined at the National Research Center for Geoanalysis, Chinese Academy of Geological Sciences, using a high-frequency infrared absorption spectrometer (HIR-944B, Wuxi High-speed Analyzer Co., Ltd., China), following the procedures described in Chu et al. (2009). The quantification limit for S was about 50 ppm.

3.2. Sr–Nd–Hf isotope analyses

Strontium, Nd, and Hf isotope compositions were determined at the State Key Laboratory of Lithospheric Evolution, IGGCAS. A combined

chemical procedure for Lu–Hf, Rb–Sr, and Sm–Nd isotopic analyses from one sample digestion was used, as described in detail by Yang et al. (2010). The Rb–Sr and Sm–Nd isotopic analyses were conducted using an Isoprobe-T thermal ionization mass spectrometer made by Isotopx Company (formerly GV instruments). Measured $^{87}Sr/^{86}Sr$ and $^{143}Nd/^{144}Nd$ ratios were corrected for mass-fractionation using $^{86}Sr/^{88}Sr = 0.1194$ and $^{146}Nd/^{144}Nd = 0.7219$, respectively. During the period of data collection, the measured values for the NBS-987 Sr standard and the JNdi-1 Nd standard were $^{87}Sr/^{86}Sr = 0.710245 \pm 16$ (2 SD, n = 8) and $^{143}Nd/^{144}Nd = 0.512117 \pm 10$ (2 SD, n = 8), respectively. Lutetium and Hf were measured using a Thermo-Fisher Neptune multicollector ICP-MS system (Yang et al., 2010). Hafnium isotopic ratios were normalized to $^{179}Hf/^{177}Hf = 0.7325$ and $^{176}Lu/^{175}Lu$ isotopic ratios were normalized using Yb isotopic ratios. During the analytical session, an Alfa Hf standard was measured 9 times and the average value of $^{176}Hf/^{177}Hf$ was 0.282181 ± 5 (2 SD). The USGS basalt reference materials BCR-2 and BHVO-2 were measured for Rb–Sr, Sm–Nd and Lu–Hf isotopic composition to monitor the accuracy of the analytical procedures; the results are in excellent agreement with the reported reference values (GeoREM, http://georem.mpch-mainz.gwdg.de/) (Table 2). The procedural blanks were about 40 pg for Rb, 300 pg for Sr, 20 pg for Sm, 60 pg for Nd, 10 pg for Lu and 40 pg for Hf, respectively.

3.3. Re–Os and PGE analyses

Re–Os isotopic compositions and PGE abundances were determined at the State Key Laboratory of Lithospheric Evolution, IGGCAS, following procedures similar to those described by Pearson and Woodland (2000).

In brief, about 2 g or 4 g of finely ground sample powder (200–400 mesh), and appropriate amounts of a mixed ^{187}Re–^{190}Os spike and a mixed ^{191}Ir–^{99}Ru–^{194}Pt–^{105}Pd spike were weighed into a clean, dry, chilled Pyrex® borosilicate glass Carius tube. For 2 g samples, 3 mL of purified concentrated HCl and 6 mL of purified concentrated HNO_3 were added to the tube, and then the tube was sealed (Shirey and Walker, 1995); for 4 g samples, the amounts of these acids were scaled up accordingly. The Carius tubes were put in a steel pressure vessel containing water to prevent the explosion of the Carius tubes, as described in detail by Qi et al. (2007). The digestions were performed at about 250 °C for 48–72 h in an oven. After opening the tubes, Os was extracted from the aqua regia solution into CCl_4 (Cohen and Waters, 1996) and then back-extracted into 4 mL of HBr; for 4 g samples, the amounts of CCl_4 and HBr used were also scaled up. The Os samples were further purified via microdistillation (Birck et al., 1997). The total procedural Os blank was 0.2–1 pg with a $^{187}Os/^{188}Os$ of about 0.16. The blank Os contribution on total Os was less than 1% for all samples and the blank correction was therefore negligible.

Rhenium, Ir, Ru, Pt and Pd remaining in aqua regia were separated from the matrix and purified first by anion exchange chromatography using 2 mL of AG 1 × 8, 100–200 mesh resin. The Re and Ru fraction was further purified using a small anion exchange column packed with 0.2 mL resin (AG 1 × 8, 100–200 mesh), whereas the Ir–Pt and Pd fractions were further purified to remove Zr and Hf using Eichrom®-LN columns. Total procedural blank was about 2–5 pg for Re, 2 pg for Ir, and 15 pg for Ru, Pt and Pd. The maximum blank corrections were <10% for low-Re samples.

Osmium isotopic compositions were measured at IGGCAS on an Isoprobe-T mass spectrometer operated in negative ion mode (Creaser et al., 1991; Volkening et al., 1991). Purified Os was loaded onto platinum filaments with $Ba(OH)_2$ as an ion emitter and measured as OsO_3^-. Most samples were measured using a single ETP multiplier in peak-jumping mode, while some samples with relatively high Os concentrations were run in static mode on Faraday cups. The measured Os isotopic ratios were corrected for mass fractionation using $^{192}Os/^{188}Os = 3.08271$ (Shirey and Walker, 1998). The in-run precisions for Os isotopic measurements were better than 0.2% (2 RSD) for all the samples. During the period of measurement of our samples, the $^{187}Os/^{188}Os$ ratio of the Johnson–Matthey standard of University of Maryland (UMD) was 0.11378 ± 4 (2 SD, n = 20) on nano-gram sized loads measured with Faraday cups and 0.1138 ± 4 (2 SD, n = 13) on 3.5–175 pg sized loads measured with the electron multiplier.

Measurements of $^{185}Re/^{187}Re$, $^{191}Ir/^{193}Ir$, $^{194}Pt/^{196}Pt$, $^{105}Pd/^{106}Pd$ and $^{99}Ru/^{101}Ru$ were conducted at IGGCAS using a Thermo-Fisher Neptune Multi-Collector ICP-MS system with an electron multiplier in peak-jumping mode or using Faraday cups in static mode, according to the measured signal intensity. The interferences of HfO (on Ir and Pt), ZrO (on Pd) were confirmed to be negligible by scanning on ^{90}Zr and ^{180}Hf peaks before sample measurement. Mass fractionation was corrected using Re, Ir, Ru, Pt, and Pd standards that were interspersed with the samples. Some Ru samples were run on the Isoprobe-T mass spectrometer in negative ion mode after a further micro-distillation purification step, following the procedures described by Becker and Walker (2003). In-run precisions for $^{185}Re/^{187}Re$, $^{191}Ir/^{193}Ir$, $^{194}Pt/^{196}Pt$, $^{105}Pd/^{106}Pd$, and $^{99}Ru/^{101}Ru$ were typically 0.1–0.5% (2 RSD).

The USGS basalt standard BHVO-2 was measured to monitor the reliability of the whole procedure. The Re, Os, Ir, Ru, Pt, and Pd concentrations and Os isotopic ratio are in agreement with the reported values (Meisel and Moser, 2004; Shinotsuka and Suzuki, 2007) (Table 3).

4. Results

4.1. Major and Trace elements

Bulk-rock major and trace element compositions are presented in Table 1. Consistent with previously reported results (Zhang et al., 1995), the WDLC and EKS basalts have high K_2O abundances ranging from 4.50 wt.% to 6.09 wt.% and K_2O/NaO ranging from 1.09 to 1.67. The SiO_2 abundances range from 49.0 to 53.5 wt.%. The MgO, CaO and Al_2O_3 abundances range from 4.45 to 9.47 wt.%, 5.09 wt.% to 7.44 wt.% and 12.2 wt.% to 14.4 wt.%, respectively. These basalts have relatively low $Mg^{\#}$ values ($100\ Mg^{2+}/(Mg^{2+}+Fe^{2+})$, falling between 61.9 and 70.6, except for sample YQ-4, having $Mg^{\#}$ value of 55.3. The loss on ignition (LOI) values range from −0.2 to 0.1 wt.%, consistent with the generally low degrees of alteration of these samples. Negative LOI values of some samples are probably due to the oxidation of FeO to Fe_2O_3 being more significant than loss of volatiles. Consistent with previous reports (Zhang et al., 1995; Zou et al., 2003; Chen et al., 2007), the WDLC and EKS basalts have relatively low CaO and particularly low Al_2O_3 at a given MgO content compared to the basalts from elsewhere in NE China (Fig. 2).

The WDLC and EKS basalts have high rare earth element (REE) and large ion lithophile element (LILE) concentrations. On a chondrite normalized REE diagram (Fig. 3a), the WDLC and EKS basalts show uniform REE characteristics with strong LREE enrichment ($(La/Yb)_N = 51.0 \pm 2.5$). The heavy REEs are also strongly fractionated with $(Sm/Yb)_N = 9.7 \pm 0.6$. These samples also have uniform primitive mantle-normalized trace element patterns (Fig. 3b), with strong LILE enrichment and pronounced enrichment of Pb and K, slight enrichment of Zr and Hf, and significant depletion of U, Th, Nb and Ta. Ce/Pb ratios of these basalts show slight variations (10.6 ± 1.3), and are much lower than the values of ocean island basalt (OIB; 25 ± 5, Hofmann et al, 1986). The La/Nb ratios of most basalts are greater than 1.2. Ba/Nb ratios range from 23 to 29.

Most WDLC and EKS basalts have low S contents, ranging from lower than 50 ppm to 100 ppm, except for a single LHS sample, LHS-6, having a S content of 140 ppm. These concentrations are much lower than those of mid-ocean ridge basalts (>1000 ppm, e.g., Gannoun et al., 2007).

4.2. Sr–Nd–Hf isotopes

The Sr and Nd isotopic compositions of the WDLC and EKS basalts are listed in Table 2. The basalt samples have relatively high $^{87}Sr/^{86}Sr$

Table 2
Rb–Sr, Sm–Nd, Lu–Hf isotopic compositions of the WDLC and EKS basalts.

Sample no.[a]	Rb (ppm)	Sr (ppm)	$^{87}Rb/^{86}Sr$	$^{87}Sr/^{86}Sr$	$2\sigma_m$	Sm (ppm)	Nd (ppm)	$^{147}Sm/^{144}Nd$	$^{143}Nd/^{144}Nd$	$2\sigma_m$	$\varepsilon_{Nd}(0)$[b]	$T_{DM}(Nd)$[c] (Ma)	Lu (ppm)	Hf (ppm)	$^{176}Lu/^{177}Hf$	$^{176}Hf/^{177}Hf$	$2\sigma_m$	$\varepsilon_{Hf}(0)$[d]	$T_{DM}(Hf)$[e]
YQ1	104	1429	0.210	0.705371	0.000012	11.09	68.03	0.09860	0.512408	0.000008	−4.5	984	0.158	12.14	0.00185	0.282564	0.000005	−7.3	995
YQ3	104	1445	0.209	0.705412	0.000008	11.16	68.52	0.09852	0.512414	0.000005	−4.4	975	0.162	12.05	0.00191	0.282549	0.000005	−7.9	1019
YQ4	104	1438	0.209	0.705370	0.000008	11.15	68.44	0.09855	0.512429	0.000008	−4.1	956	0.167	12.20	0.00195	0.282574	0.000004	−7.0	985
YQ6	105	1447	0.210	0.705383	0.000011	11.20	68.85	0.09838	0.512428	0.000005	−4.1	956	0.173	12.20	0.00202	0.282572	0.000004	−7.1	988
YQ7	106	1449	0.211	0.705439	0.000012	11.20	68.80	0.09843	0.512423	0.000005	−4.2	963	0.158	12.19	0.00184	0.282570	0.000004	−7.1	986
YQ8	105	1448	0.210	0.705420	0.000012	11.20	68.87	0.09836	0.512439	0.000004	−3.9	941	0.171	12.21	0.00199	0.282569	0.000005	−7.2	993
LHS-1	106	1441	0.212	0.705410	0.000008	11.13	68.50	0.09825	0.512407	0.000005	−4.5	982	0.170	11.82	0.00205	0.282563	0.000004	−7.4	1003
LHS-3	106	1438	0.214	0.705414	0.000014	11.11	68.23	0.09849	0.512399	0.000006	−4.7	995	0.161	11.77	0.00194	0.282553	0.000005	−7.7	1014
LHS-4	112	1448	0.223	0.705579	0.000008	11.00	68.06	0.09772	0.512400	0.000005	−4.6	987	0.170	11.98	0.00202	0.282512	0.000005	−9.2	1076
LHS-6	87.7	1733	0.146	0.705133	0.000010	13.66	82.66	0.09994	0.512464	0.000004	−3.4	921	0.191	8.896	0.00305	0.282661	0.000006	−3.9	884
LHS-6R	88.0	1733	0.147	0.705151	0.000007	13.64	82.54	0.1000	0.512453	0.000005	−3.6	935	0.189	8.893	0.00302	0.282656	0.000006	−4.1	892
HSS-2	93.9	1567	0.173	0.705184	0.000008	12.06	72.08	0.1012	0.512474	0.000005	−3.2	918	0.167	8.748	0.00272	0.282659	0.000006	−4.0	879
HSS-2R	93.7	1564	0.173	0.705133	0.000008	12.06	72.06	0.1012	0.512461	0.000006	−3.5	935	0.176	8.718	0.00287	0.282657	0.000007	−4.1	886
HSS-5	91.9	1626	0.163	0.705130	0.000008	12.46	74.45	0.1012	0.512453	0.000006	−3.6	946	0.182	8.743	0.00296	0.282657	0.000005	−4.1	889
HSS-6	94.8	1330	0.206	0.705273	0.000008	10.33	61.65	0.1013	0.512432	0.000004	−4.0	975	0.167	9.620	0.00247	0.282616	0.000006	−5.5	937
HSS-8	95.2	1297	0.212	0.705241	0.000012	10.38	61.68	0.1017	0.512418	0.000004	−4.3	998	0.167	9.608	0.00248	0.282617	0.000006	−5.5	935
KD-1	106	1541	0.199	0.705589	0.000008	10.84	67.91	0.09656	0.512362	0.000005	−5.4	1026	0.163	12.68	0.00182	0.282522	0.000006	−8.9	1056
KD-3	103	1581	0.188	0.705657	0.000011	10.21	63.58	0.09708	0.512342	0.000007	−5.8	1057	0.163	–	–	–	–	–	–
KD-4	105	1581	0.192	0.705637	0.000010	10.18	63.35	0.09718	0.512344	0.000006	−5.7	1055	0.164	11.42	0.00204	0.282524	0.000006	−8.8	1058
KD-5	103	1574	0.190	0.705626	0.000007	10.36	64.58	0.09698	0.512347	0.000006	−5.7	1050	0.162	11.36	0.00203	0.282521	0.000005	−8.9	1064
BCR-2 measured	46.9	340.2	0.398	0.705010	0.000011	6.563	28.68	0.1384	0.512664	0.000005			0.520	4.942	0.0150	0.282878	0.000007		
BCR-2 reported[f]	46.9	340		0.705000		6.58	28.7		0.512636				0.503	4.9		0.282878			
BHVO-2 measured	9.13	395.8	0.0667	0.703491	0.000007	6.081	24.52	0.1500	0.513002	0.000010			0.275	4.444	0.00880	0.283103	0.000007		
BHVO-2 reported[f]	9.11	396		0.703469		6.07	24.5		0.512980				0.274	4.36		0.283109			

[a] R, replicate analysis.
[b] $\varepsilon_{Nd}(0)$ values were calculated using $(^{143}Nd/^{144}Nd)_{CHUR(0)} = 0.512638$.
[c] $T_{DM}(Nd)$ values were calculated using $(^{147}Sm/^{144}Nd)_{DM(0)} = 0.2137$ and $(^{143}Nd/^{144}Nd)_{DM(0)} = 0.513151$.
[d] $\varepsilon_{Hf}(0)$ values were calculated using $(^{176}Hf/^{177}Hf)_{CHUR(0)} = 0.282772$.
[e] $T_{DM}(Hf)$ values were calculated using $(^{176}Lu/^{177}Hf)_{DM(0)} = 0.0384$ and $(^{176}Hf/^{177}Hf)_{DM(0)} = 0.28325$.
[f] Reported values for the reference materials are from GeoREM (http://georem.mpch-mainz.gwdg.de/).

Table 3
Re–Os isotopic compositions of the WDLC and EKS basalts.[a]

Sample[b]		Re (ppb)	Os (ppb)	$^{187}Re/^{188}Os$	$^{187}Os/^{188}Os$	$2\sigma_m$	[c]γ_{Os}	Ir (ppb)	Ru (ppb)	Pt (ppb)	Pd (ppb)	$(Pd/Ir)_N$
YQ-1		0.079	0.067	5.68	0.15098	0.00024	18.9	0.0498	0.121	0.245	0.078	1.3
YQ-1R		0.070	0.062	5.48	0.15081	0.00010	18.7	0.0622	0.131	0.338	0.108	1.4
YQ-3		0.029	0.068	2.08	0.16975	0.00034	33.7	0.0248	0.115	0.712	0.110	3.7
YQ-4		0.022	0.054	1.97	0.14388	0.00016	13.3	0.0410	0.092	0.507	0.105	2.1
YQ-4R		0.033	0.101	1.57	0.14227	0.00009	12.0	0.0961	0.212	0.325	0.087	0.8
YQ-6		0.021	0.088	1.16	0.15325	0.00031	20.7	0.0273	0.103	0.471	0.087	2.6
YQ-7		0.019	0.147	0.631	0.14082	0.00027	10.9	0.1136	0.271	0.565	0.093	0.7
YQ-7R		0.014	0.094	0.746	0.15881	0.00008	25.1	0.0679	0.147	0.317	0.108	1.3
YQ-8		0.019	0.289	0.321	0.12954	0.00031	2.0	0.0578	0.209	0.424	0.074	1.1
LHS-1		0.025	0.111	1.10	0.13629	0.00022	7.3	0.0674	0.146	0.280	0.162	2.0
LHS-3		0.017	0.132	0.619	0.13112	0.00013	3.2	0.1195	0.198	0.311	0.192	1.3
LHS-4		0.074	0.113	3.17	0.13490	0.00016	6.2	0.0935	0.199	0.357	0.243	2.1
LHS-6		0.895	1.55	2.77	0.11869	0.00002	−6.5	0.2823	0.285	0.677	0.295	0.9
LHS-6R		0.068	0.389	0.846	0.12447	0.00007	−2.0	0.0465	0.100	0.941	0.273	4.9
HSS-2		0.059	0.033	8.72	0.14713	0.00026	15.8	0.0390	0.093	0.240	0.143	3.0
HSS-5		0.064	0.029	10.8	0.16294	0.00033	28.3	0.0244	0.052	0.243	0.114	3.9
HSS-6		0.036	0.105	1.65	0.14017	0.00016	10.4	0.0994	0.334	0.285	0.203	1.7
HSS-6R		0.074	0.238	1.51	0.12997	0.00011	2.3	0.1214	0.364	0.971	0.279	1.9
HSS-8		0.102	0.114	4.32	0.13666	0.00049	7.6	0.0815	0.204	0.416	0.145	1.5
KD-1		0.121	0.0818	7.11	0.13706	0.00016	7.9	0.0275	0.117	0.345	0.084	2.5
KD-3		0.109	0.177	2.95	0.12709	0.00006	0.1	0.0955	0.247	0.643	0.061	0.5
KD-4		0.0888	0.0676	6.34	0.13590	0.00023	7.0	0.0319	0.139	0.502	0.057	1.5
KD-5		0.130	0.133	4.70	0.13023	0.00014	2.5	0.0574	0.149	0.355	0.112	1.6
BHVO-2	1	0.511	0.118	21.1	0.14625	0.00005		0.0764	0.132	12.0	2.58	
Measured	2	0.544	0.122	21.6	0.14609	0.00008		0.0809	0.138	8.47	2.67	
BHVO-2 Reported[d]	Ref. 1	0.543	0.101	–	–	–		0.058	0.129	10.1	2.94	
	Ref. 2	0.523	0.115	–	–	–		0.710	0.123	7.39	2.99	

[a] All the Re, Os, Ir, Ru, Pt, Pd concentration and the Os isotopic composition data are blank-corrected.
[b] R—Replicate analysis.
[c] γ_{Os} values were calculated using $(^{187}Os/^{188}Os)_{CHUR(0)} = 0.1270$ (Shirey and Walker, 1998).
[d] Reported values for the reference material BHVO-2: Ref. 1, Meisel and Moser, 2004; Ref. 2, Shinotsuka and Suzuki, 2007.

ratios varying between 0.7051 and 0.7057. The $^{143}Nd/^{144}Nd$ ratios range from 0.5123 to 0.5125. The Sr–Nd isotopes of the WDLC and EKS basalts are more evolved (i.e., Sr isotopic compositions are more radiogenic and Nd isotopic compositions are less radiogenic) than those of mantle xenoliths carried in nearby Keluo basalts (Zhang et al., 2000, 2011) and Cenozoic basalts elsewhere in NE China (e.g., Chen et al., 2007; Yan and Zhao, 2008) (Fig. 4a). The $T_{DM}(Nd)$ model ages of these basalts range from 918 to 1057 Ma. Consistent with previously reported results (Zhang et al., 1995; Zou et al., 2003), $^{87}Sr/^{86}Sr$ correlates negatively with $^{143}Nd/^{144}Nd$, demonstrating Sr–Nd isotope systematics similar to EM1 (Zindler and Hart, 1986) (Fig. 4a).

The Lu–Hf isotopic compositions of the WDLC and EKS basalts are also listed in Table 2. The Lu/Hf ratios range from 0.0018 to 0.0030, which are far lower than the value for modern chondrite (0.0332, Blichert-Toft and Albarède, 1997). The $^{176}Hf/^{177}Hf$ ratios vary from 0.2825 to 0.2827 (Table 2; Fig. 4b). In term of Hf isotopes, the WDLC and EKS basalts are also more evolved (i.e., have less radiogenic Hf isotopic compositions) than the mantle xenoliths they host (Zhang et al., 2011) (Fig. 4b). Similar to Nd model ages, these basalts give uniform $T_{DM}(Hf)$ model ages ranging from 879 to 1076 Ma. On the Hf–Nd isotopic correlation diagram, no obvious Hf–Nd decoupling is seen when compared to MORB or OIB (Fig. 4b).

4.3. Re–Os isotopes

Re–Os isotope data for the WDLC and EKS basalts are given in Table 3. In general, compared with Cenozoic basalts from other intraplate localities such as Columbia River, Hannuoba, South-Eastern (SE) Australia and Central Europe (Chesley and Ruiz, 1998; McBride et al., 2001; Jiang and Zhi, 2010; Jung et al., 2011), the WDLC and EKS basalts have higher Os and lower Re contents (Fig. 5a). Most samples have Re concentrations less than 0.1 ppb. The only exception is one analysis of sample LHS-6, giving Re concentrations of 0.895 ppb. The WDLC and EKS samples have Os concentrations ranging from 0.029 ppb to greater than 0.2 ppb. One analysis of sample LHS-6 gives extremely high Os concentration (1.55 ppb).

The $^{187}Os/^{188}Os$ values of most samples range from 0.13 to 0.17, which overlaps with the $^{187}Os/^{188}Os$ ranges of OIB basalts summarized in Shirey and Walker (1998) and Harvey et al. (2011), and MORB glass (e.g., Alard et al., 2005). The only exception is the high Os concentration sample LHS-6. Two analyses of this sample yield low $^{187}Os/^{188}Os$ values of 0.1187 and 0.1245, respectively. As shown in Fig. 5b, compared with the Cenozoic continental basalts from Hannuoba, SE Australia and Central Europe (Chesley and Ruiz, 1998; McBride et al., 2001; Jiang and Zhi, 2010; Jung et al., 2011), the WDLC and EKS potassic basalts generally have much lower age-corrected $^{187}Os/^{188}Os$ ratios.

Replicate analyses of some WDLC and EKS basalts (Table 3) not only rarely gave reproducible Re and Os concentrations, but also failed to reproduce $^{187}Os/^{188}Os$ ratios. Especially, replicate analyses of sample LHS-6 gave highly heterogeneous Re and Os concentrations, and Os isotopic ratio. The higher $^{187}Os/^{188}Os$ ratio of sample LHS-6R relative to LHS-6 corresponds with a lower Os concentration.

4.4. Platinum-group elements (PGE)

PGE data for the WDLC and EKS basalts are presented in Table 3. In general, the WDLC and EKS basalts have low PGE abundances, ranging from 0.0244 to 0.282 ppb for Ir, 0.0525 to 0.364 ppb for Ru, 0.240 to 0.971 ppb for Pt, and 0.0571 to 0.295 ppb for Pd. Similar to the Re and Os concentration measurements, the PGE abundances in replicate analyses of some samples also vary considerably, far beyond analytical uncertainties (Table 3). Despite this, as shown in Fig. 6, the chondrite-normalized PGE patterns (and hence PGE element ratios) are generally reproducible. The WDLC and EKS basalts show only slight PPGE enrichment relative to IPGE ($(Pd/Ir)_N = 1.9 \pm 1.1$) (Table 3). Exceptionally, consistent with its un-radiogenic Os, sample LHS-6 has relatively high Ir and Os concentrations relative to Pt and Pd (Fig. 6). Additionally,

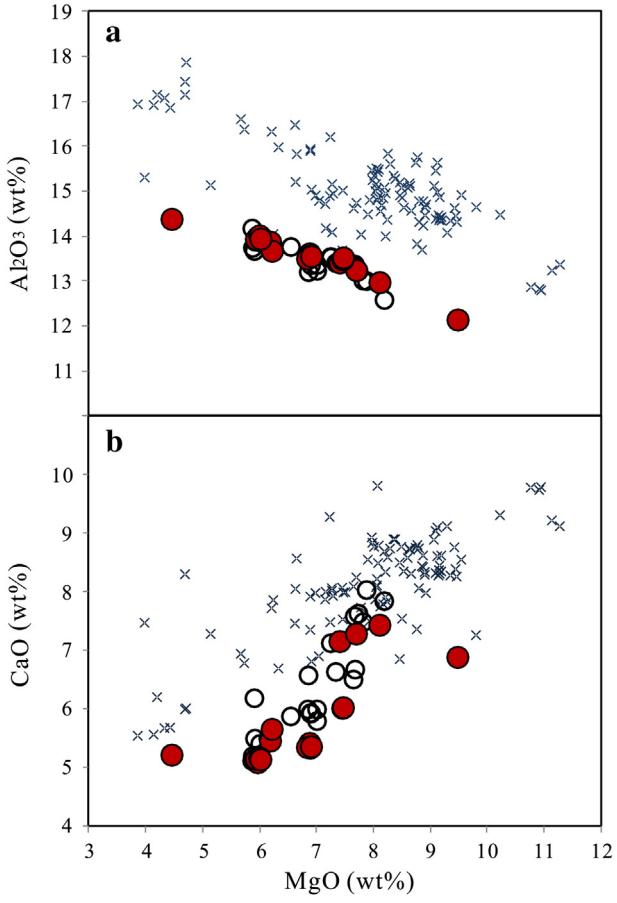

Fig. 2. Al_2O_3 vs MgO (a) and CaO vs MgO (b) for WDLC and EKS basalts. Solid circles: this study; Open circles: WDLC and EKS data from Zou et al. (2003) and Chen et al. (2007); Crosses: data for basalts from NE China elsewhere (Chen et al., 2007; Yan and Zhao, 2008).

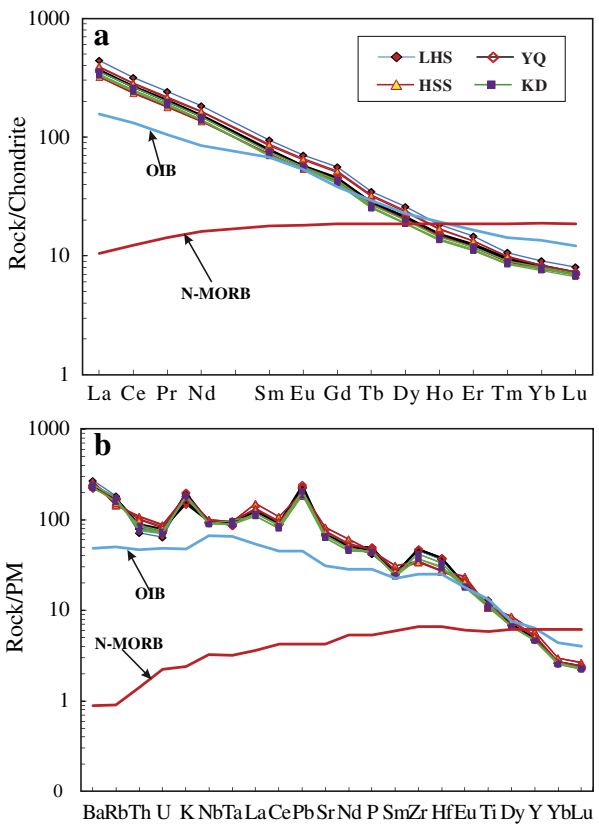

Fig. 3. Chondrite-normalized rare earth element patterns (a) and primitive mantle-normalized trace element patterns (b) for the WDLC and EKS basalts. Chondrite normalizing values are from Masuda et al. (1973) divided by 1.2; Data for OIB, N-MORB and primitive mantle are from McDonough and Sun (1995).

sample LHS-6 and LHS-6R (particularly LHS-6) have elevated Os/Ru and Os/Ir ratios compared to those of the other samples.

5. Discussion

5.1. PGE and Os isotope heterogeneity in the WDLC and EKS basalts

Mantle sulphides and refractory PGE-rich alloys have parts-per-million (ppm) to weight percentage (wt.%) concentrations of PGE (e.g., Lorand and Alard, 2001; Walker et al., 2002; Pearson et al., 2004; Lorand et al., 2010, 2013), making them prime candidates for a source of a possible "nugget effect". For example, a 20 μg mantle sulphide with an Os concentration of 20 ppm (e.g., Alard et al., 2000, 2002; Pearson et al., 2002; Harvey et al., 2006, 2010, 2011; Lorand et al., 2013) contains twice as much Os as 2 g of basalt with an Os concentration of 100 ppt. Therefore, the heterogeneous distribution of a component that contains anomalously high Os (+PGE) abundances throughout the sampled rock powder could account for the observed heterogeneities in replicate basalt analyses (Table 3). Although no discrete sulphide or PGE alloy grains have been observed in the WDLC and EKS basalts, a "nugget effect" due to incorporation of such mantle phases during the ascent of basalt through the SCLM should be considered. Indeed, the inclusions enclosed in xenocrystic material in basaltic lavas have been previously suggested as a mechanism to account for unradiogenic $^{187}Os/^{188}Os$ and elevated Os concentrations (e.g., Widom et al., 1999; Jackson and Shirey, 2011).

Although analyzed samples of the WDLC and EKS basalts were hand-picked to avoid obvious xenolith debris, microprobe analyses of olivine "phenocrysts" showed that minor proportions of the olivines are mantle xenocrysts (i.e., a few olivine grains from samples LHS-4 and KD-4 have Fo > 90, CaO < 0.10 wt.% (Table S1), cf., Sobolev et al., 2007; Jackson and Shirey, 2011). Any sulphides hosted within xenocrystic grains (e.g., Burton et al., 1999) would not have the opportunity to become dispersed within a larger volume of melt. If its host was not recognized as xenocrystic at the time of basalt preparation, this could readily account for the elevated Os (+IPGE) abundance and unradiogenic $^{187}Os/^{188}Os$ in some WDLC and EKS samples, especially for LHS-6. Moreover, the WDLC and EKS basalts with relatively high Ni and S content have the highest Os concentrations and least radiogenic Os isotopic compositions (Fig. 7a–d), also consistent with the incorporation of sulphide. Since it is possible that refractory alloys could be mechanically transported in an ascending melt (e.g., Ballhaus et al., 2006), the heterogeneous distribution of refractory alloys may also be possible to cause the "nugget effect" in WDLC and EKS samples. This is supported by the relatively low Pt and Pd concentrations relative to Ir and Ru in these samples compared to OIB and MORB (especially LHS-6) (Fig. 6). In addition, Cr-spinel xenocrysts, of probable mantle origin, are observed in sample LHS-4 (Fig. S1b). Although spinel itself is more Os-rich than silicate mantle phases (Burton et al., 1999; Harvey et al., 2010, 2011), it is unlikely to account for a significant proportion of mantle-derived PGE itself. Consequently, it appears that sulphides or PGE alloys enclosed in xenocrysts are the most likely candidates for the heterogeneity for PGE concentrations and Os isotopic compositions in the WDLC and EKS basalt.

Although the incorporation of moderately radiogenic, interstitial metasomatic sulphides from the SCLM also seems to be a plausible source of heterogeneity, in all likelihood those sulphides would be dissolved by a S-undersaturated melt (Reisberg et al., 2005; Sen et al., 2011) and its PGE budget homogenized within a relatively large volume of melt compared to the volume of sulphide dissolved. It seems that this

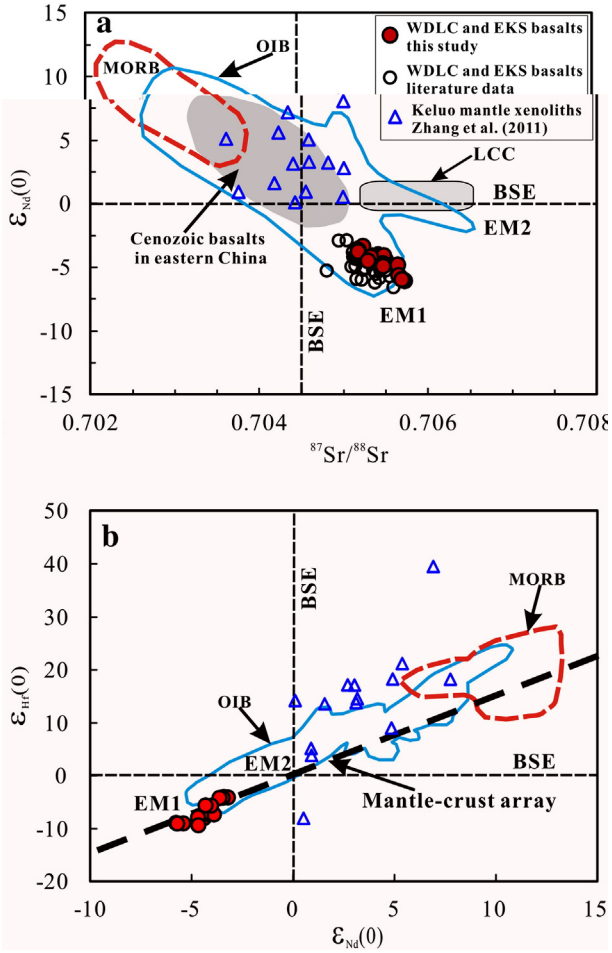

Fig. 4. Sr–Nd (a) and Hf–Nd (b) isotope diagrams for WDLC and EKS basalts. In (a): literature data for WLDC and EKS basalts are from Peng et al. (1986), Basu et al. (1991), Zhang et al. (1995, 1998) and Zou et al. (2003); Field for lower continental crust (LCC) in WDLC and EKS area is based on Wu et al. (2003). Field for Cenozoic basalts in eastern China is based on Chen et al. (2007) and Yan and Zhao (2008); MORB, OIB, BSE, EM1 and EM2 end members are from Zindler and Hart (1986). In (b): MORB and OIB fields are based on Salters and White (1998); the bulk Earth $^{176}Hf/^{177}Hf$ value (BSE) and the mantle–crust array are based on Blichert-Toft and Albarède (1997).

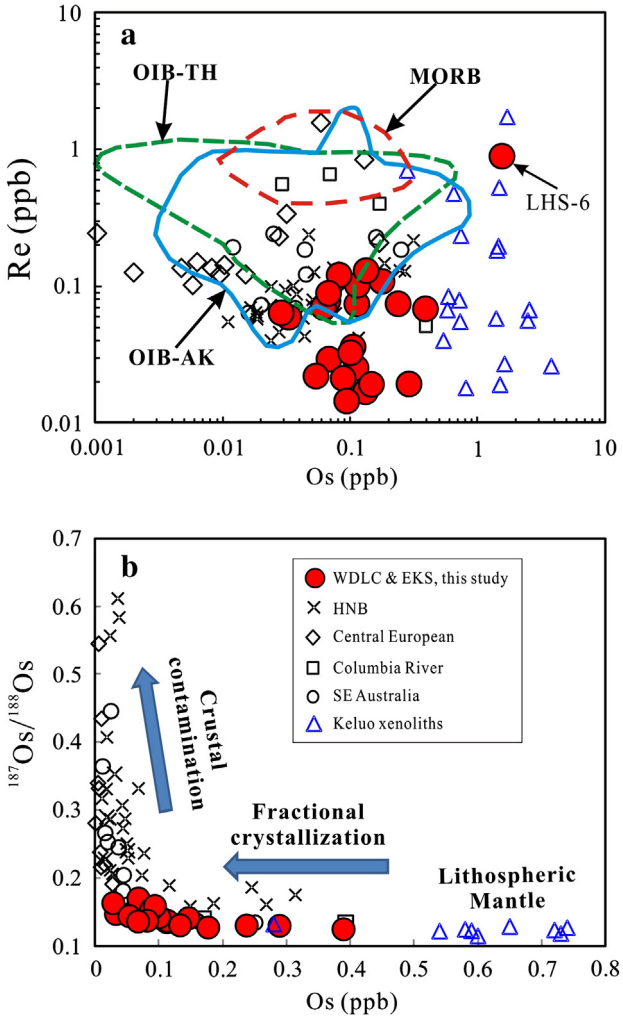

Fig. 5. Re vs. Os (a) and Os concentration vs. $^{187}Os/^{188}Os$ (b) variation diagrams. Data sources: Central European (Jung et al., 2011); HNB, Hannuoba (Jiang and Zhi, 2010); SE Australia (McBride et al., 2001); Columbia River (Chesley and Ruiz, 1998); Keluo mantle xenoliths (Zhang et al., 2011); MORB and OIB fields are from Shirey and Walker (1998): OIB TH, ocean island basalt tholeiites; OIB AB, ocean island alkali basalts. In (b): Samples with Os > 0.8 ppb are not plotted for clarity; $^{187}Os/^{188}Os$ ratios are all age-corrected values.

process would not account for the PGE heterogeneity between different powder splits of the same sample.

5.2. Crustal contamination

Since basaltic magmas have high concentrations of lithophile elements, Sr–Nd–Pb–Hf isotopes and lithophile elements are not particularly sensitive to minor crustal contamination. This will be especially true for the LILE- and LREE- rich WDLC and EKS basalts. However, even minor amounts of crustal contamination have the potential to significantly alter the Os isotopic composition of a basaltic magma with low Os concentrations (cf., Lassiter and Luhr, 2001; McBride et al., 2001; Xu et al., 2007; Qi and Zhou, 2008; Jung et al., 2011). It is possible that some of the low Os WDLC and EKS basalts have been affected by crustal contamination during magma ascent, in particular, at degrees that are not easily detected using lithophile elements. Therefore, the $^{187}Os/^{188}Os$ and PGE systematics of the WDLC and EKS basalts potentially allow this small degree of crustal contamination to be quantified.

As argued above, it is possible that some WDLC and EKS basalts have incorporated some primary sulphides (sulphides enclosed in silicate minerals, i.e., Os-rich, Re-poor, evolving in low-Re environment and preserving unradiogenic osmium isotope ratios) or PGE alloys of SCLM origin during magma ascent. Moreover, most of these basalts have relatively low MgO contents (Table 1) and are thus unlikely to be primary melts, suggesting that Os concentrations in the WDLC and EKS basalts were also likely to be strongly affected by differentiation. Consequently, it is likely that the basaltic magmas arrived in the crust with a range of Os concentrations. As a result, it is difficult to constrain the degree of crustal contamination by assimilation–fractional crystallization (AFC) modeling (DePaolo, 1981). Nevertheless, as shown in Fig. 8, there is a significant covariation between $^{187}Os/^{188}Os$ and 1/Os ($R^2 = 0.47$), demonstrating that it seems likely that the WDLC and EKS basalts have been affected by minor crustal contamination during magma ascent. Normally, an Os isotope ratio c. 0.128 is considered to be representative of the parental basaltic magma as suggested by previous studies (e.g., McBride et al., 2001; Xu et al., 2007; Jiang and Zhi, 2010; Jung et al., 2011). Therefore, we assume the parental magma of the WDLC and EKS basalts to have roughly a $^{187}Os/^{188}Os$ of c. 0.128, but with varying Os concentrations (about 0.03–1.6 ppb, based on samples analyzed in this study, Table 3) when they arrive in the lower crust. Consequently, if an Os isotope ratio of 0.8 and Os concentration of 49 ppt is taken as being representative of the lower crust (Saal et al., 1998; Chesley et al., 2002), the degree of crustal contamination observed in the WDLC and EKS basalts can be modeled by simple binary mixing. It is found that the addition of

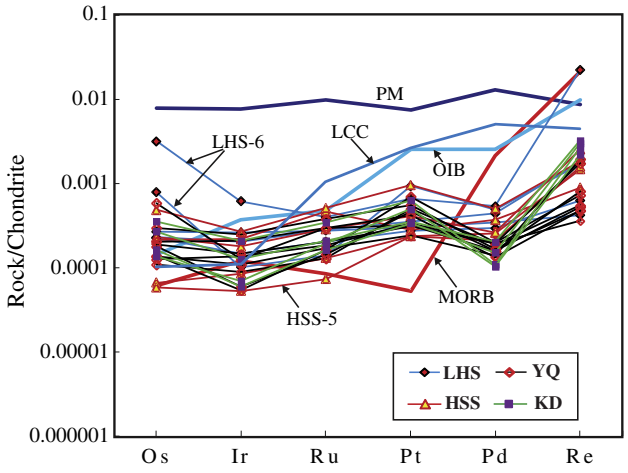

Fig. 6. Chondrite-normalized PGE patterns for WDLC and EKS basalts. Chondrite values are from McDonough and Sun (1995). Primitive mantle (PM) values are based on Becker et al. (2006). Data for OIB-Canary Island alkali basalts with calculated parental melt of 12 wt.% MgO, and MORB are based on Day (2013) and references therein. LCC (lower continental crust) values are based on Rudnick and Gao (2003).

about only 3.5% of lower crust can replicate the observed covariation between $^{187}Os/^{188}Os$ and 1/Os ($R^2 = 0.47$; Fig. 8) fairly well. Nonetheless, as shown in Fig. 8, it is possible that some samples, especially from different volcanoes, have experienced different degrees of crustal contamination ranging from 2% to 8%. The rough correlation between the Pd/Ir and $^{187}Os/^{188}Os$ (Fig. 9) ($R^2 = 0.39$) is also consistent with minor crustal contamination in some basaltic melts, since the samples with high Pd/Ir ratios are a result of low Ir contents, not high Pd contents.

Nevertheless, there remains the possibility that some samples with radiogenic Os isotopes, which plot above the line for 3.5% of crustal contamination, result from preferential melting of interstitial sulphides (sulphides occurred along boundary of mineral grains, Re-rich, Os-poor, evolving in high-Re environment and having variable and radiogenic osmium isotope ratios) in a metasomatized mantle source (Alard et al., 2005; Schulte et al., 2009; Harvey et al., 2011) and/or the addition of minor SCLM-derived interstitial sulphides during magma ascent (e.g., Sen et al., 2011). This is particularly true for the YQ samples, as reflected by their radiogenic Os but relatively high Os concentrations. However, we still prefer that the YQ samples have experienced a larger degree of crustal contamination since their Pd contents are low. In contrast, the samples which plot below the line for 3.5% crustal contamination are probably due to the incorporation of SCLM-primary sulphides.

Addition of minor amounts (2–8%) of lower crust would not have much effect on incompatible elements and Sr–Nd–Pb–Hf isotopic ratios for the LILE- and LREE-rich WDLC and EKS basalts. For example, if we assume the local lower crust having Nd concentration of 20 ppm (Rudnick and Gao, 2003) and $^{143}Nd/^{144}Nd$ of 0.51265 (Wu et al., 2003), 8% contamination of lower crust only shift the $^{143}Nd/^{144}Nd$ of the WDLC and EKS basalts of about 0.000007. Similarly, incorporation of primary mantle sulphides or the addition of metasomatized sulphides would also have negligible effect on the lithophile element systems and Sr–Nd–Pb–Hf isotopes. As a result, no correlation exists between Os isotopic compositions and incompatible trace element ratios such as Ce/Pb and La/Nb, and Sr or Nd or Hf isotopic compositions (not shown); indeed, there are very limited variations in Sr–Nd–Hf isotopes and Ce/Pb and La/Nb ratios, especially for YQ samples (Tables 1 and 2).

5.3. Source of the WDLC and EKS basalts—SCLM vs. asthenosphere

It is highly debated that the EM1-like features of the Cenozoic basalts in NE China originated from either the SCLM or the asthenospheric mantle (e.g., Song et al., 1990; Basu et al., 1991; Zhang et al., 1995; Zou et al., 2003; Choi et al., 2006; Xu et al., 2012; Kuritani et al., 2013). Based on the highly potassic, LREE and LILE-enriched trace elemental characteristics, the strong fractionation of the heavy REE (HREE), low Al_2O_3 content at a given MgO, significant excesses in ^{230}Th, and Sr–Nd–Pb isotopic characteristics, Zhang et al. (1995) and Zou et al. (2003) suggested that the WDLC and EKS basalts were likely produced

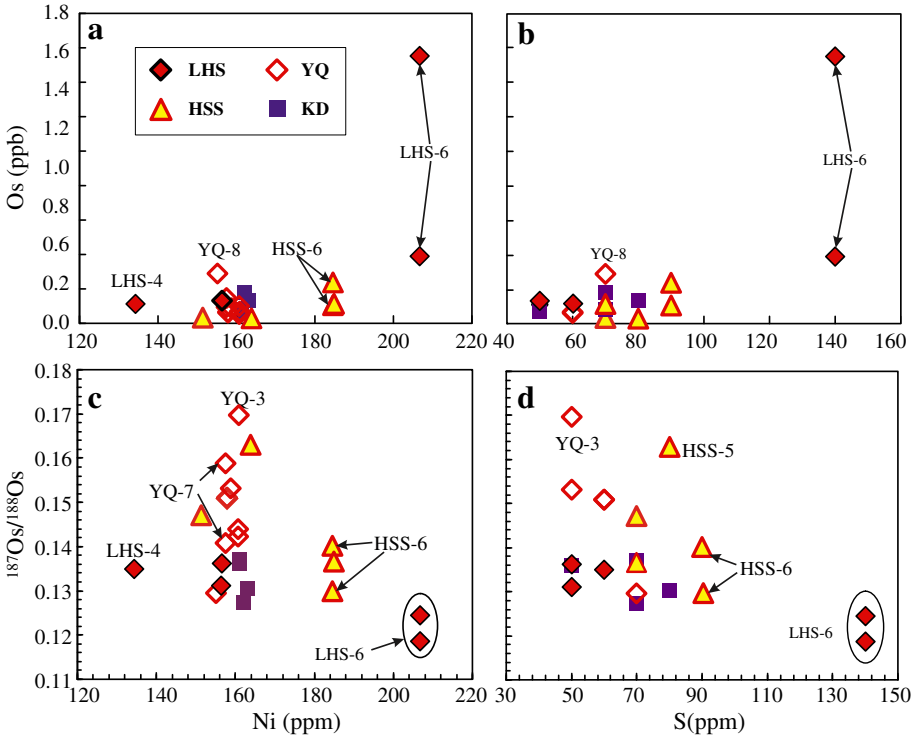

Fig. 7. Diagrams of Os concentration vs. Ni content (a), Os concentration vs. S content (b), $^{187}Os/^{188}Os$ vs. Ni content (c) and $^{187}Os/^{188}Os$ vs. S content (d) for WDLC and EKS basalts.

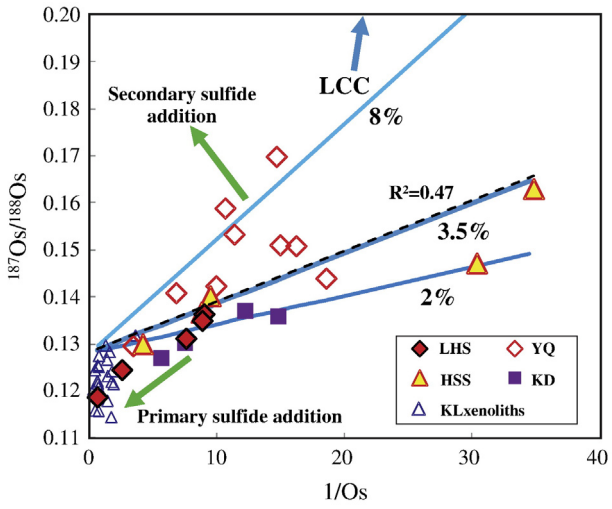

Fig. 8. $^{187}Os/^{188}Os$ vs. 1/Os. The solid lines represent binary mixing lines modeled as follows: (1) basaltic magma arrived in the crust with variable Os concentrations (about 0.03–1.6 ppb, based on samples analyzed in this study) but similar Os isotopic compositions (we assume $^{187}Os/^{188}Os = 0.128$); (2) addition of 2%, 3.5% and 8% of lower crust ($^{187}Os/^{188}Os = 0.8$ and Os concentration = 49 ppt, Saal et al., 1998) to the basaltic magma. The line for addition of 3.5% of lower crust is consistent with the regression line (the dashed line, $R^2 = 0.47$) for data points from all the volcanoes. The arrows show the trends for addition of lower continental crust (LCC), secondary sulphides and primary sulphides.

by small-degree melting of phlogopite-bearing garnet peridotite in metasomatized SCLM. The presence of garnet constrains the depth of the magma source to 80–120 km (Zou et al., 2003). However, several studies have suggested that delaminated cratonic lithosphere from eastern China may exist locally in the shallow asthenosphere beneath NE China (e.g., Xu et al., 2005; Choi et al., 2006) and that basalts from this region may preserve evidence for re-melting of this reservoir. They argued that the asthenospheric mantle beneath eastern Asian is characterized by two distinct, large-scale domains—one a mixture of DMM and EM1 components, and the other a mixture of DMM and EM2. More recently, some authors (Xu et al., 2012; Kuritani et al., 2013) argued that the Cenozoic basalts in NE China originated from an asthenospheric mantle source containing recycled oceanic crust materials. They suggest that the subducted Pacific slab (Huang and Zhao, 2006) and/or the stagnant ancient Pacific slab (Kuritani et al., 2011) in the mantle transition zone have contributed to the Cenozoic magmatism in NE China. This is reasonable as the re-melting of upwelling asthenospheric mantle containing recycled oceanic or lower continental crust has widely been invoked to account for the evolved Sr–Nd–Hf isotopic composition of intraplate basalts (e.g., Sobolev et al., 2007; Chen et al., 2009; Zhang et al., 2009; Xu et al., 2012).

As discussed above, crustal contamination has not played an important role in the formation of the WDLC and EKS basalts. Therefore, consistent with previous studies (Zhang et al., 1995; Zou et al., 2003), data obtained in this study, including low Al_2O_3 content at a given MgO (Fig. 2a), high K content, LREE and LILE-enriched trace elemental characteristics (Fig. 3a, b), particularly strong fractionation of the heavy REE ($(Sm/Yb)_N = 9.7 \pm 0.6$), EM1-like Sr–Nd–Hf isotopic characteristics (Fig. 4a, b), all suggest that the WDLC and EKS basalts mainly originated from a phlogopite-bearing garnet peridotite in the SCLM. The presence of phlogopite and rutile in some Keluo and WDLC xenoliths (Zhang et al., 2000, 2011) also supports that the SCLM beneath WEK area has been metasomatized by K-rich silicate melt.

In the model involving delaminated ancient SCLM from eastern China that exists locally in the asthenosphere beneath NE China (Choi et al., 2006), amphibole and phlogopite will breakdown at high pressure (>3 GPa) and are thus not considered to be stable in the asthenospheric mantle (Class and Goldstein, 1997). Moreover, a delaminated ancient SCLM from eastern China is also unlikely to be the source material for the EM1-like signature because the delaminated Archaean SCLM beneath eastern China does not have an EM1-like composition (e.g., Chu et al., 2009 and references therein). Therefore, it seems plausible that phlogopite-bearing metasomatized SCLM rather than an asthenospheric source containing fragments of delaminated ancient cratonic mantle may provide a source for the WDLC and EKS high-K basalts (Fig. 9).

In the model that the potassic- and EM1-like natures of the basalts originated from the mantle transition zone, which has been metasomatized by K-rich sediment-derived fluids ~1.5 Ga ago through the stagnation of an ancient slab and further recent hydration by the stagnation of the subducted Pacific slab (Kuritani et al., 2013), it is difficult to envision such a process because of the great distance (>2000 km) between the WEK provinces and the active Pacific subduction zone (Japan Arc) (Zhang et al., 1998; Zou et al., 2003) in western NE China. Significant ^{230}Th enrichments in WDLC basalts also suggest that the source rocks were not metasomatized by fluids released during recent (<350 ka) subduction of Pacific sediments (Zou et al., 2003). Furthermore, it has long been recognized that LILEs, such as Ba, Rb, and Sr are fluid-mobile and have elevated concentrations in sub-arc environments, while fluid-immobile elements such as Nb and Ta, are largely unaffected by contributions of fluids from the subducting slab (Arculus and Powell, 1986). A mantle source which has been metasomatized by a subduction-related fluid would be enriched in radiogenic Os (Brandon et al., 1996; Widom et al., 2003). Due to the effect of preferential melting of metasomatic components for Os isotopes (e.g., Harvey et al., 2011; Sen et al., 2011), melting of such a mantle source would produce melts with slightly increasing $^{187}Os/^{188}Os$ along with increasing Ba/Nb (Chesley et al., 2002). Such a trend is absent in the WDLC and EKS basalts (Fig. 10). In contrast, some samples especially YQ samples with high $^{187}Os/^{188}Os$ have relatively low Ba/Nb ratios. In fact, the WDLC and EKS basalts have very low Ba/Nb ratios with limited variability (23–29).

Consequently, it seems most likely that the WDLC and EKS mainly originated from low degree melting of a SCLM source metasomatized by an EM1-like signature, rather than an EM1 signature asthenospheric mantle source.

In terms of Os isotopes, the WDLC and EKS basalts generally have unradiogenic to moderately radiogenic Os isotopic compositions ($^{187}Os/^{188}Os = 0.1187–0.17$). In principle these relatively OIB-like Os isotopic values are not inconsistent with an asthenospheric origin (Liu et al., 2008; Harvey et al., 2011). However, as discussed before, the measured Os isotope ratios cannot be attributed solely to the

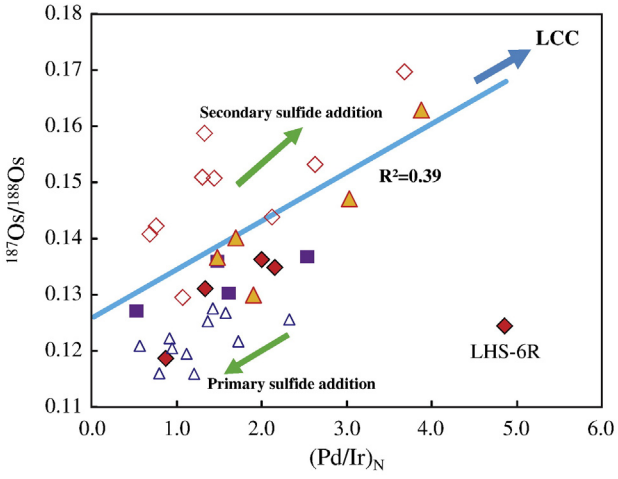

Fig. 9. $^{187}Os/^{188}Os$ vs. $(Pd/Ir)_N$ for WDLC and EKS basalts. The solid line denotes the regression line for all the data points except for LHS-6R. Symbols and arrows as in Fig. 8. The Os isotopic composition and $(Pd/Ir)_N$ of LCC are about 0.8 (Saal et al., 1998) and 46 (Rudnick and Gao, 2003), repectively.

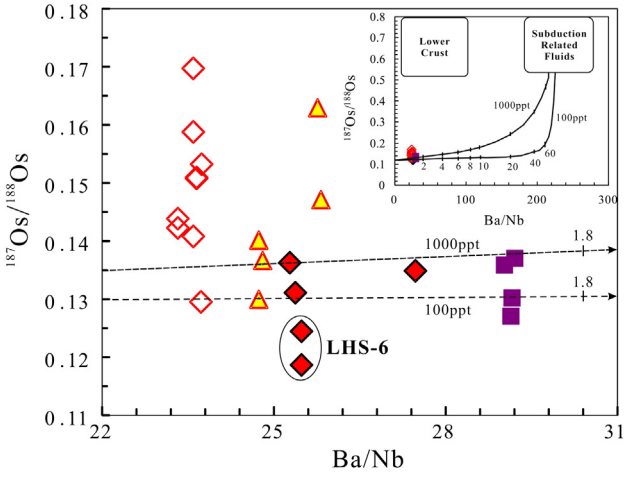

Fig. 10. $^{187}Os/^{188}Os$ vs. Ba/Nb for WDLC and EKS basalts. Symbols as in Fig. 8. Trends for contamination of mantle source of basalts by subduction-related fluids, fields of Ba/Nb and $^{187}Os/^{188}Os$ for the subduction fluids and the lower crust based are based on Chesley et al. (2002). Numbers along trend lines represent percentage of fluid required to influence the mantle source. Large numbers along trend lines represent the Os in ppt for subduction-related fluids used in the two-component mixing model (the mantle source of WDLC and EKS basalts is assumed to be 1000 ppt). The real trend should possibly toward more radiogenic Os along with increasing Bb/Nb ratios due to the effect of preferential melting of metasomatic components in mantle source for Os isotopes (e.g., Harvey et al., 2011).

mantle reservoir from which the basalts were produced. Most of the $^{187}Os/^{188}Os$ values have been elevated by up to 2–8% crustal contamination and/or the effects of incorporating metasomatic sulphide en route to the surface, while the most unradiogenic values may be deceptively low because of the incorporation of xenocryst-hosted primary sulphide. Similarly, the relative flat PGE patterns ($(Pd/Ir)_N = 1.9 \pm 1.1$) compared to MORB and OIB (Fig. 6) could indicate the contribution of a SCLM source for the WDLC and EKS basalts and, like Os isotope ratios, can also be interpreted in a number of ways. Therefore, notwithstanding the clear utility of Os isotopes and PGE in fingerprinting the sources of basalts that have not experienced complex histories (cf., Shirey and Walker, 1998; Day, 2013), these tools do not unequivocally distinguish between an asthenospheric and a lithospheric source for the WDLC and EKS basalts.

5.4. Nature of the SCLM underlying the WEK area

As discussed above, the WDLC and EKS basalts mainly originated from the underlying SCLM. Despite this, as the WDLC and EKS basalts have more evolved Sr–Nd–Hf isotopic signatures than those of mantle xenoliths carried in nearby Keluo highly potassic basalts (Zhang et al., 2011) (Fig. 4a, b), the role of peridotite with the composition similar to that of Keluo xenoliths can be largely discounted in the petrogenesis of the WDLC and EKS basalts. Moreover, since the Keluo xenoliths mainly comprise spinel lherzolites and harzburgites with minor dunites and wehrlites, they should have been located in the SCLM above the source of the WDLC and EKS basalts (garnet peridotites). Therefore, it is possible that the lithospheric mantle underlying the WEK area is layered, at least in terms of Sr–Nd–Hf isotopes, i.e., the lower part of lithospheric mantle (the potential source of the WDLC and EKS basalts) has more radiogenic Sr and less radiogenic Nd and Hf than the upper part of lithospheric mantle (represented by the Keluo mantle xenoliths), despite their similar Nd and Hf model ages (Zhang et al., 2000) (Table 2).

The crustal growth in XMOB during the Phanerozoic is significant, as reflected by the radiogenic Nd–Hf isotopic compositions of granites in the area (e.g., Wu et al., 2003; Zhang et al., 2010), while the potassic rocks originating from the underlying SCLM have EM1-like Sr–Nd–Hf isotopic signatures as demonstrated above. This suggests that the SCLM beneath the WEK area is decoupled from the overlying crust. Previous studies argued that the SCLM beneath the Phanerozoic XMOB is ancient and have been metasomatised extensively by SiO_2-undersaturated potassic magma that was likely generated from low-degree partial melting of deep asthenosphere during the Proterozoic (Zhang et al., 1995, 2000; Zou et al., 2003; Zhang et al., 2011).

EM1-like signatures of the WDLC and EKS basalts cannot be owed to metasomtism by melts derived from subducted oceanic crust related to the closure of the Paleo-Asian Ocean in the Paleozoic and Paleo-Pacific Ocean during the Mesozoic. Their isotopic compositions fall outsides the range for those of oceanic basalts and MORB that are believed to be derived primarily from the asthenospheric mantle. Especially, the very unradiogenic Pb isotopic signatures of the potassic rocks ($^{206}Pb/^{204}Pb = 16.3–17.3$), which require a long-term residence (>2 Ga) of low U/Pb in the mantle source, indicate that at least the Pb isotopic signatures of the WEK basalts cannot be attributed to modifications by Phanerozoic subduction events in the region (Zhang et al., 1998). On the other hand, the partial melting of peridotite cannot cause a large U/Pb fractionation and, therefore, the melt generated from low-degree partial melting of asthenosphere cannot have a significantly different U/Pb ratio from that of the depleted mantle (Kuritani et al., 2013). Therefore, it is also difficult to derive the very unradiogenic Pb isotopic signatures of the potassic rocks ($^{206}Pb/^{204}Pb = 16.3–17.3$) with the model presented by Zhang et al. (1995) and Zou et al. (2003).

As lower continental crust is known to be depleted in U relative to Pb (e.g., Rudnick and Gao, 2003), given enough time it will develop unradiogenic Pb isotopic compositons. Consequently, based on low Ce/Pb (~9.4–13.5) and EM1-like Sr–Nd–Hf isotopic signatures, in conjugation with low Pb isotope ratios ($^{206}Pb/^{204}Pb = 16.61$ to 17.06) as reported by Zhang et al. (1995) and Zou et al. (2003), different from the previous studies (Zhang et al., 1995, 1998; Zou et al., 2003; Kuritani et al., 2013), we suggest that the mantle source of WDLC and EKS basalts have been metasomatised by recycled old lower continental crust materials (i.e., an EM1-like signature). It is likely that some pyroxenite would be formed in the SCLM if mantle peridotite was metasomatised by melt containing a contribution from lower crustal materials (e.g., Xu, 2002). Some pyroxenite xenoliths were found in WEK basalts (Zhang et al., 2000), consistent with such an explanation. This is also supported by the relatively low CaO abundance at a given MgO (Fig. 2b) for the WDLC and EKS basalts, as melts of pyroxenite are generally low in CaO owing to the dominant effect of residual clinopyroxene (e.g., Herzberg, 2011).

It is likely that the present lower crust in XMOB is significantly different from earlier crust at this locality. As there are probably some Precambrian fragments present in NE China (Wu et al., 2003; Meng et al., 2010), it is likely that the original crust in WEK area was old. It is possible that the original lower crust together with SCLM foundered probably during lithospheric thinning in eastern China that started in the Mesozoic. The delamination of the old lower crust is probably related to the multiple subduction events in this region. Subsequently, the newly-formed SCLM beneath the WEK area was metasomatised by melt contributed from the delaminated lower crust. The whole SCLM beneath the WEK area was extensively and contemporaneously metasomtised as reflected by the similar Nd (Hf) model age between the mantle xenoliths (Zhang et al., 2000, 2011) and the potassic basalts (Table 2) in this area. It is possible that the lower part of the SCLM have been affected more strongly than the upper part of the SCLM. This metasomatism leads to the SCLM underlying the WEK area having more radiogenic Sr and less radiogenic Nd and Hf isotopic compositions than the overlying Phanerozoic crust.

Conclusively, consistent with previous studies (Zhang et al., 1995, 1998; Zou et al., 2003), we suggest that the WDLC and EKS basalts originated from phlogopite-bearing garnet peridotite within the SCLM. During low degree of the partial melting of the SCLM, metasomatic components such as phlogopites are easily melted and their high-K characteristics exported into the WDLC and EKS basalts (Zou et al., 2003).

In contrast, garnet is mainly retained in the mantle source. This leads to significant ^{230}Th excess in the WDLC and EKS basalts (Zou et al., 2003). Similarly, hafnium isotopes could uniquely trace contributions from the SCLM if melts are derived from garnet-bearing SCLM (Jung et al., 2011). Given sufficient time, the strong increase of Lu/Hf relative to Sm/Nd in mantle with significant garnet would result in trends that deviate from the crust–mantle Hf–Nd isotope array, towards radiogenic ^{176}Hf/^{177}Hf at a given ^{143}Nd/^{144}Nd (e.g., Salters and Zindler, 1995; Bizimis et al., 2007; Chen et al., 2009). However, the WDLC and EKS potassic lavas have very low Lu/Hf ratios (Table 2) and do not show Hf–Nd isotope decoupling on Hf–Nd correlation diagrams (Fig. 4b). This also indicates a low degree melting of the phlogopite-bearing garnet peridotites, and consequently the Lu–Hf isotopic signature of garnet in the SCLM has not been exported into the resulting basaltic magma.

6. Concluding remarks

(1) The WDLC and EKS highly potassic basalts show uniform REE and trace elemental characteristics and relatively homogeneous Sr–Nd–Hf isotopic compositions, but heterogeneous Os isotopic compositions ranging from 0.1187 to ~0.17. It is possible that some samples with radiogenic Os isotopic compositions may have been contaminated by minor amounts of lower crustal materials, while other samples, with un-radiogenic Os isotopic compositions, may have incorporated small amounts of mantle materials such as xenocryst-hosted primary sulphides and/or PGE micro-alloys during magma ascent through the overlying SCLM. Both the correlation between the ^{187}Os/^{188}Os and 1/Os, and the positive correlation between ^{187}Os/^{188}Os and Pd/Ir are consistent with these scenarios. In contrast, the minor crustal contamination and incorporation of sulphides in the SCLM have an insignificant influence on the lithophile elements and Sr–Nd–Hf isotopic compositions.

(2) The strong enrichments of LREE and LILE, and EM1 like Sr–Nd–Hf isotopic characteristics suggest that the WDLC and EKS highly potassic basalts mainly originated from metasomatized SCLM. Combined with the WDLC and EKS basalts having Ce/Pb ratios (~9.4–13.5) much lower than typical OIB and MORB, and low ^{206}Pb/^{204}Pb ratios, it seems likely that the source of WDLC and EKS basalts is SCLM that has been metasomatized by delaminated old lower continental crust materials. Furthermore, since the WDLC and EKS basalts have more radiogenic Sr and less radiogenic Nd–Hf isotopic compositions than the SCLM xenoliths carried in nearby Keluo highly potassic basalts, the lithospheric mantle underlying the Wudalianchi–Erkeshan–Keluo (WEK) area is likely layered, at least in terms of Sr–Nd–Hf isotopes.

Supplementary data to this article can be found online at http://dx.doi.org/10.1016/j.chemgeo.2013.08.007.

Acknowledgments

Roberta Rudnick, Richard Walker, Hong Zhong, Lihui Chen, Yanjie Tang and Jifeng Ying are sincerely thanked for helpful discussions and constructive suggestions. Yan-Bin Zhang, He Li, Jie Cao, Hongyue Wang, Dingshuai Xue, Qian Mao and Yuguang Ma are thanked for their help on ICP-MS, XRF and EPMA analysis. This work was financially supported by National Natural Science Foundation of China (NSFC Grants 40873008, 41273018 and 41273021) and the Institute of Geology and Geophysics, Chinese Academy of Sciences (IGGCAS Grant ZC1002). Yigang Xu (reviewer), an anonymous reviewer and Laurie Reisberg (editor) are sincerely thanked for their constructive comments which greatly improve the quality of this manuscript.

References

Alard, O., Griffin, W.L., Lorand, J.-P., Jackson, S.E., O'Reilly, S.Y., 2000. Nonchondritic distribution of the highly siderophile elements in mantle sulphides. Nature 407, 891–894.
Alard, O., Griffin, W.L., Pearson, N.J., Lorand, J.-P., O'Reilly, S.Y., 2002. New insights into the Re–Os systematics of subcontinental lithospheric mantle from in-situ analysis of sulphides. Earth Planet. Sci. Lett. 203, 651–663.
Alard, O., Luguet, A., Pearson, N.J., Griffin, W.L., Lorand, J.-P., Gannoun, A., Burton, K.W., O'Reilly, S.Y., 2005. In-situ Os isotopes in abyssal peridotites bridge the isotopic gap between MORBs and their source mantle. Nature 436, 1005–1008.
Arculus, R.J., Powell, R., 1986. Source component mixing in the regions of arc magma generation. J. Geophys. Res. 91, 5913–5926.
Ballhaus, C., Bockrath, C., Wohlgemuth-Ueberwasser, C., Vera Laurenz, V., Berndt, J., 2006. Fractionation of the noble metals by physical processes. Contrib. Mineral. Petrol. 152, 667–684.
Basu, A.R., Wang, J.W., Huang, W.K., Xie, G.H., Tatsumoto, M., 1991. Major element, REE, and Pb, Nd and Sr isotopic geochemistry of Cenozoic volcanic rocks of eastern China: implications for their origin from suboceanic-type mantle reservoirs. Earth Planet. Sci. Lett. 105, 149–169.
Becker, H., Walker, R.J., 2003. In search of extant Tc in the early solar system: ^{98}Ru and ^{99}Ru abundances in iron meteorites and chondrites. Chem. Geol. 196, 43–56.
Becker, H., Horan, M.F., Walker, R.J., Gao, S., Lorand, J.-P., Rudnick, R.L., 2006. Highly siderophile element composition of the Earth's primitive upper mantle: constraints from new data on peridotite massifs and xenoliths. Geochim. Cosmochim. Acta 70, 4528–4550.
Birck, J.L., Roy-Barman, M., Capmas, F., 1997. Re–Os isotopic measurements at the femtomole level in natural samples. Geostand. Newslett. 20, 19–27.
Bizimis, M., Griselin, M., Lassiter, J.C., Salters, V.J.M., Sen, G., 2007. Ancient recycled mantle lithosphere in the Hawaiian plume: osmium–hafnium isotopic evidence from peridotite mantle xenoliths. Earth Planet. Sci. Lett. 257, 259–273.
Blichert-Toft, J., Albarède, F., 1997. The Lu–Hf geochemistry of chondrites and the evolution of the mantle–crust system. Earth Planet. Sci. Lett. 148, 243–258.
Brandon, A.D., Creaser, R.A., Shirey, S.B., Carlson, R.W., 1996. Os recycling in subduction zones. Science 272, 861–864.
Burton, K.W., Schiano, P., Birck, J.-L., Allègre, C.J., 1999. Osmium isotope disequilibrium between mantle minerals in a spinel–lherzolite. Earth Planet. Sci. Lett. 172, 311–322.
Chen, Y., Zhang, Y.X., Graham, D., Su, S.G., Deng, J.F., 2007. Geochemistry of Cenozoic basalts and mantle xenoliths in Northeast China. Lithos 96, 108–126.
Chen, L.H., Zeng, G., Jiang, S.Y., Hofmann, A.W., Xu, X.S., 2009. Sources of Anfengshan basalts: subducted lower crust in the Sulu UHP belt, China. Earth Planet. Sci. Lett. 286, 426–435.
Chesley, J.T., Ruiz, J., 1998. Crust–mantle interaction in large igneous provinces: implications from the Re–Os isotope systematics of the Columbia River flood basalts. Earth Planet. Sci. Lett. 154, 1–11.
Chesley, J.T., Ruiz, J., Righter, K., Ferrari, L., Gomez-Tuena, A., 2002. Source contamination versus assimilation: an example from the Trans-Mexican Volcanic Arc. Earth Planet. Sci. Lett. 195, 211–221.
Chesley, J.T., Righter, K., Ruiz, J., 2004. Large-scale mantle metasomatism: a Re–Os perspective. Earth Planet. Sci. Lett. 219, 49–60.
Choi, S.H., Mukasa, S.B., Kwon, S.-T., Andronikov, A.V., 2006. Sr, Nd, Pb and Hf isotopic compositions of late Cenozoic alkali basalts in South Korea: evidence for mixing between the two dominant asthenospheric mantle domains beneath East Asia. Chem. Geol. 232, 134–151.
Chu, Z.Y., Wu, F.Y., Walker, R.J., Rudnick, R.L., Pitcher, L., Puchtel, I.S., Yang, Y.H., Wilde, S.A., 2009. Temporal evolution of the lithospheric mantle beneath the eastern North China Craton. J. Petrol. 50, 1857–1898.
Class, C., Goldstein, S.L., 1997. Plume–lithosphere interactions in the ocean basins: constraints from the source mineralogy. Earth Planet. Sci. Lett. 150, 245–260.
Cohen, A.S., Waters, F.G., 1996. Separation of osmium from geological materials by solvent extraction for analysis by TIMS. Anal. Chim. Acta 332, 269–275.
Creaser, R.A., Papanastassiou, D.A., Wasserburg, G.J., 1991. Negative thermal ion mass spectrometry of osmium, rhenium, and iridium. Geochim. Cosmochim. Acta 55, 397–401.
Day, J.M.D., 2013. Hotspot volcanism and highly siderophile elements. Chem. Geol. 341, 50–74.
DePaolo, D., 1981. Trace element and isotopic effects of combined wallrock assimilation and fractional crystallization. Earth Planet. Sci. Lett. 53, 189–202.
Douglass, J., Schilling, J.-G., Fontignie, D., 1999. Plume–ridge interactions of the Discovery and Shona mantle plumes with the southern Mid-Atlantic Ridge (40°–55°S). J. Geophys. Res. 107, 2941–2962.
Fan, Q., Hooper, P.R., 1991. The Cenozoic basaltic rocks of eastern China: petrology and chemical composition. J. Petrol. 32, 765–810.
Flower, M., Tamaki, K., Hoang, N., 1998. Mantle extrusion: a model for dispersed volcanism and DUPAL-like asthenosphere in East Asia and the Western Pacific. In: Flower, M., Chung, S.-L., Lo, C.-H., Lee, T.Y. (Eds.), Mantle dynamics and plate interactions in East Asia. Am. Geophys. Union, Geophys. Monogr., vol. 27, pp. 67–88.
Gannoun, A., Burton, K.W., Parkinson, I.J., Alard, O., Schiano, P., Thomas, L.E., 2007. The scale and origin of the osmium isotope variations in mid-ocean ridge basalts. Earth Planet. Sci. Lett. 259, 541–556.
Hart, S.R., Hauri, E.H., Oschmann, L.A., Whitehead, J.A., 1992. Mantle plumes and entrainment—isotopic evidence. Science 256, 517–520.
Harvey, J., Gannoun, A., Burton, K.W., Rogers, N.W., Alard, O., Parkinson, I.J., 2006. Ancient melt extraction from the oceanic upper mantle revealed by Re–Os isotopes in abyssal peridotites from the Mid-Atlantic ridge. Earth Planet. Sci. Lett. 244, 606–621.
Harvey, J., Gannoun, A., Burton, K.W., Schiano, P., Rogers, N.W., Alard, O., 2010. Unravelling the effects of melt depletion and secondary infiltration on mantle

Re–Os isotopes beneath the French Massif Central. Geochim. Cosmochim. Acta 74, 293–320.
Harvey, J., Dale, C.W., Gannoun, A., Burton, K.W., 2011. Osmium mass balance in peridotite and the effects of mantle-derived sulphides on basalt petrogenesis. Geochim. Cosmochim. Acta 75, 5574–5596.
Herzberg, C., 2011. Identification of source lithology in the Hawaiian and Canary Islands: implications for origins. J. Petrol. 52, 113–146.
Hofmann, A.W., Jochum, K.P., Seufer, M., White, W.M., 1986. Nb and Pb in oceanic basalts: new constraints on mantle evolution. Earth Planet. Sci. Lett. 79, 33–45.
Huang, J.L., Zhao, D.P., 2006. High-resolution mantle tomography of China and surrounding regions. J. Geophys. Res. 111 (B09305).
Jackson, M.G., Shirey, S.B., 2011. Re–Os isotope systematics in Samoan shield lavas and the use of Os-isotopes in olivine phenocrysts to determine primary magmatic compositions. Earth Planet. Sci. Lett. 312, 91–101.
Jiang, L., Zhi, X.C., 2010. Re–Os isotope geochemistry of basalts from Hannuoba, North China: evidence for Re volatile loss and crust–mantle interaction (in Chinese with English abstract). Acta Petrol. Sin. 26, 1265–1276.
Jung, S., Pfänder, J.A., Brauns, M., Maas, R., 2011. Crustal contamination and mantle source characteristics in continental intra-plate volcanic rocks: Pb, Hf and Os isotopes from central European volcanic province basalts. Geochim. Cosmochim. Acta 75, 2664–2683.
Kuritani, T., Ohtani, E., Kimura, J.-I., 2011. Intensive hydration of the mantle transition zone beneath China caused by ancient slab stagnation. Nat. Geosci. 4, 713–716.
Kuritani, T., Kimura, J.-I., Ohtani, E., Miyamoto, H., Furuyama, K., 2013. Transition zone origin of potassic basalts from Wudalianchi volcano, northeast China. Lithos 156–159, 1–12.
Lassiter, J.C., Luhr, J.F., 2001. Osmium abundance and isotope variations in mafic Mexican volcanic rocks: evidence for crustal contamination and constraints on the geochemical behavior of osmium during partial melting and fractional crystallization. Geochem. Geophys. Geosyst. 2. http://dx.doi.org/10.1029/2000GC000116.
Liu, C.Q., Masuda, A., Xie, G.H., 1994. Major- and trace-element compositions of Cenozoic basalts in east China: petrogenesis and mantle source. Chem. Geol. 114, 19–42.
Liu, J.Q., Han, J.T., Fyfe, W.S., 2001. Cenozoic episodic volcanism and continental rifting in northeast China and possible link to Japan Sea development as revealed from K–Ar geochronology. Tectonophysics 339, 385–401.
Liu, C.Z., Snow, J.E., Hellebrand, E., Brugmann, G., von der Handt, A., Buchl, A., Hofmann, A.W., 2008. Ancient, highly heterogeneous mantle beneath Gakkel ridge, Arctic Ocean. Nature 452, 311–316.
Lorand, J.-P., Alard, O., 2001. Platinum-group element abundances in the upper mantle: new constraints from in situ and whole-rock analyses of Massif Central xenoliths (France). Geochim. Cosmochim. Acta 65, 2789–2806.
Lorand, J.-P., Alard, O., Luguet, A., 2010. Platinum-group element micronuggets and refertilization process in the Lherz peridotite. Earth Planet. Sci. Lett. 289, 298–310.
Lorand, J.-P., Luguet, A., Alard, O., 2013. Platinum-group element systematics and petrogenetic processing of the continental upper mantle: a review. Lithos 164–167, 2–21.
Masuda, A., Nakamura, N., Tanaka, T., 1973. Fine structures of mutually normalised rare-earth patterns of chondrites. Geochim. Cosmochim. Acta 37, 239–244.
McBride, J.S., Lambert, D.D., Nicholls, I.A., Price, R.C., 2001. Osmium isotopic evidence for crust–mantle interaction in the genesis of continental intraplate basalts from the Newer Volcanics Province, Southeastern Australia. J. Petrol. 42, 1197–1218.
McDonough, W.F., Sun, S.S., 1995. The composition of the Earth. Chem. Geol. 120, 223–253.
Meisel, T., Moser, J., 2004. Platinum-group element and rhenium concentrations in low abundance reference materials. Geostand. Geoanal. Res. 28, 233–250.
Meng, E., Xu, W.L., Pei, F.P., Yu, Y., Zhang, X.Z., 2010. Detrital-zircon geochronology of Late Paleozoic sedimentary rocks in eastern Heilongjiang Province, NE China: implications for the tectonic evolution of the eastern segment of the Central Asian Orogenic Belt. Tectonophysics 485, 42–51.
Pearson, D.G., Woodland, S.J., 2000. Solvent extraction/anion exchange separation and determination of PGEs (Os, Ir, Pt, Pd, Ru) and Re–Os isotopes in geological samples by isotope dilution ICP-MS. Chem. Geol. 165, 87–107.
Pearson, N.J., Alard, O., Griffin, W.L., Jackson, S.E., O'Reilly, S.Y., 2002. In situ measurement of Re–Os isotopes in mantle sulphides by laser-ablation multi-collector inductively coupled plasma mass spectrometry: analytical methods and preliminary results. Geochim. Cosmochim. Acta 66, 1037–1050.
Pearson, D.G., Irvine, G.J., Ionov, D.A., Boyd, F.R., Dreibus, G.E., 2004. Re–Os isotope systematics and platinum group element fractionation during mantle melt extraction: a study of massif and xenolith peridotite suites. Chem. Geol. 208, 29–59.
Peng, Z.C., Zartman, R.E., Futa, K., Chen, D.G., 1986. Pb-, Sr- and Nd-isotopic systematics and chemical characteristics of Cenozoic basalts, Eastern China. Chem. Geol. 59, 3–33.
Phipps Morgan, J., Morgan, W.J., 1999. Two-stage melting and the geochemical evolution of the mantle: a recipe for mantle plum-pudding. Earth Planet. Sci. Lett. 170, 215–239.
Qi, L., Zhou, M.-F., 2008. Platinum-group element and Sr–Nd–Os isotope geochemistry of Permian Emeishan flood basalts, in Guizhou Province, SW China. Chem. Geol. 248, 83–103.
Qi, L., Zhou, M.F., Wang, C.Y., Sun, M., 2007. Evaluation of the determination of Re and PGEs abundances of geological samples by ICP-MS coupled with a modified Carius tube digestion at different temperatures. Geochem. J. 41, 407–414.
Reisberg, L., Zhi, X., Lorand, J.P., Wagner, C., Peng, Z., Zimmermann, C., 2005. Re–Os and S systematics of spinel peridotite xenoliths from east central China: evidence for contrasting effects of melt percolation. Earth Planet. Sci. Lett. 239, 286–308.
Rudnick, R.L., Gao, S., 2003. Composition of the continental crust. In: Rudnick, R.L. (Ed.), Treatise on Geochemistry. Elsevier, pp. 1–64.
Rudnick, R.L., Walker, R.J., 2009. Interpreting ages from Re–Os isotopes in peridotites. Lithos 112, 1083–1095.
Saal, A.E., Rudnick, R.L., Ravizza, G.E., Hart, S.R., 1998. Re–Os isotope evidence for the composition, formation and age of the lower continental crust. Nature 393, 58–61.
Salters, V.J.M., White, W.M., 1998. Hf isotope constraint on mantle evolution. Chem. Geol. 145, 447–460.
Salters, V.J.M., Zindler, A., 1995. Extreme $^{176}Hf/^{177}Hf$ in the sub-oceanic mantle. Earth Planet. Sci. Lett. 129, 13–30.
Schulte, R.F., Schilling, M., Anma, R., Farquhar, J., Horan, M.F., Komiya, T., Piccoli, P.M., Pitcher, L., Walker, R.J., 2009. Chemical and chronologic complexity in the convecting upper mantle: evidence from the Taitao ophiolite, southern Chile. Geochim. Cosmochim. Acta 73, 5793–5819.
Sen, I.S., Bizimis, M., Sen, G., Huang, S., 2011. A radiogenic Os component in the oceanic lithosphere? Constraints from Hawaiian pyroxenite xenoliths. Geochim. Cosmochim. Acta 75, 4899–4916.
Sengör, A., Natal'lin, B.A., Burtaman, V.S., 1993. Evolution of the Altaid tectonic collage and Palaeozoic crustal growth in Eurasia. Nature 364, 299–307.
Shinotsuka, K., Suzuki, K., 2007. Simultaneous determination of platinum group elements and rhenium in rock samples using isotope dilution inductively coupled plasma mass spectrometry after cation exchange separation followed by solvent extraction. Anal. Chim. Acta 603, 129–139.
Shirey, S.B., Walker, R.J., 1995. Carius tube digestions for low blank rhenium–osmium analysis. Anal. Chem. 67, 2136–2141.
Shirey, S.B., Walker, R.J., 1998. The Re–Os isotope system in cosmochemistry and high temperature geochemistry. Annu. Rev. Earth Planet. Sci. 26, 423–500.
Sobolev, A.V., Hofmann, A.W., Kuzmin, D.V., Yaxley, G.M., Arndt, N.T., Chung, S.-L., Danyushevsky, L.V., Elliott, T., Frey, F.A., Garcia, M.O., Gurenko, A.A., Kamenetsky, V.S., Kerr, A.C., Krivolutskaya, N.A., Matvienkov, V.V., Nikogosian, I.K., Rocholl, A., Sigurdsson, I.A., Sushchevskaya, N.M., Teklay, M., 2007. The amount of recycled crust in mantle-derived melts. Science 316, 412–417.
Song, Y., Frey, F.A., Zhi, X., 1990. Isotopic characteristics of Hannuoba basalts, eastern China: implications for their petrogenesis and the composition of subcontinental mantle. Chem. Geol. 85, 35–62.
Volkening, J., Walczyk, T., Heumann, K., 1991. Os isotope ratio determinations by negative thermal ionisation mass spectrometry. Int. J. Mass Spectrom. Ion Process. 105, 147–159.
Walker, R.J., Pitchard, H.M., Ishiwatari, A., Pimentel, M., 2002. The osmium isotopic composition of convecting upper mantle deduced from ophiolite chromites. Geochim. Cosmochim. Acta 66, 329–345.
Widom, E., Hoernle, K.A., Shirey, S.B., Schmincke, H.-U., 1999. Os isotope systematic in the Canary Islands and Madeira: lithospheric contamination and mantle plume signatures. J. Petrol. 40, 297–314.
Widom, E., Kepezhinskas, P., Defant, M., 2003. The nature of metasomatism in the sub-arc mantle wedge: evidence from Re–Os isotopes in Kamchatka peridotite xenoliths. Chem. Geol. 196, 283–306.
Wu, F.Y., Jahn, B.M., Wilde, S.A., Lo, C.H., Yui, T.F., Lin, Q., Ge, W.C., Sun, D.Y., 2003. Highly fractionated I-type granites in NE China (II): isotopic geochemistry and implications for crustal growth in the Phanerozoic. Lithos 67, 191–204.
Xu, Y.G., 2002. Evidence for crustal components in mantle source and constraints on recycling mechanism: pyroxenite xenoliths from Hannuoba, North China. Chem. Geol. 182, 301–322.
Xu, Y.G., Ma, J.L., Frey, F.A., Feigenson, M.D., Liu, J.F., 2005. Role of lithosphere–asthenosphere interaction in the genesis of Quaternary alkali and tholeiitic basalts from Datong, western North China Craton. Chem. Geol. 224, 247–271.
Xu, J.F., Suzuki, K., Xu, Y.G., Mei, H.J., Li, J., 2007. Os, Pb, and Nd isotope geochemistry of the Permian Emeishan continental flood basalts: insights into the source of a large igneous province. Geochim. Cosmochim. Acta 71, 2104–2119.
Xu, Y.G., Zhang, H.H., Qiu, H.N., Ge, W.C., Wu, F.Y., 2012. Oceanic crust components in continental basalts from Shuangliao, Northeast China: derived from the mantle transition zone? Chem. Geol. 328, 168–184.
Yan, J., Zhao, J.X., 2008. Cenozoic alkali basalts from Jingpohu, NE China: the role of lithosphere–asthenosphere interaction. J. Asian Earth Sci. 33, 106–121.
Yang, Y.H., Zhang, H.F., Chu, Z.Y., Xie, L.W., Wu, F.Y., 2010. Combined chemical separation of Lu, Hf, Rb, Sr, Sm and Nd from a single rock digest and precise and accurate isotope determinations of Lu–Hf, Rb–Sr and Sm–Nd isotope systems using Multi-Collector ICP-MS and TIMS. Int. J. Mass Spectrom. 290, 120–126.
Zhang, M., Menzies, M.A., Suddaby, P., Thirlwall, M.F., 1991. EM1 signature from the post-Archaean subcontinental lithospheric mantle: isotopic evidence from the potassic volcanic rocks in NE China. Geochem. J. 25, 387–398.
Zhang, M., Suddaby, P., Thompson, R.N., Thirlwall, M.F., Menzies, M.A., 1995. Potassic volcanic rocks in NE China: geochemical constraints on mantle source and magma genesis. J. Petrol. 36, 1275–1303.
Zhang, M., Zhou, X.H., Zhang, J.B., 1998. Nature of the lithospheric mantle beneath NE China: evidence from potassic volcanic rocks and mantle xenoliths. In: Flower, M., Chung, S.-L., Lo, C.-H., Lee, T.Y. (Eds.), Mantle Dynamics and Plate Interactions in East Asia. Am. Geophys. Union, Geophys. Monogr., vol. 27, pp. 197–219.
Zhang, M., Suddaby, P., O'Reilly, S.Y., Norman, M., Qiu, J., 2000. Nature of the lithospheric mantle beneath the eastern part of the Central Asian fold belt: mantle xenolith evidence. Tectonophysics 328, 131–156.
Zhang, J.J., Zheng, Y.F., Zhao, Z.F., 2009. Geochemical evidence for interaction between oceanic crust and lithospheric mantle in the origin of Cenozoic continental basalts in east-central China. Lithos 110, 305–326.
Zhang, Y.L., Ge, W.C., Gao, Y., Chen, J.S., Zhao, L., 2010. Zircon U–Pb ages and Hf isotopes of granites in Longzhen area and their geological implications. Acta Petrol. Sin. 26, 1059–1073 (in Chinese with English abstract).
Zhang, Y.L., Liu, C.Z., Ge, W.C., Wu, F.Y., Chu, Z.Y., 2011. Ancient sub-continental lithospheric mantle (SCLM) beneath the eastern part of the Central Asian

Orogenic Belt (CAOB): implications for crust–mantle decoupling. Lithos 126, 233–247.
Zhi, X.C., Song, Y., Frey, F.A., Feng, J.L., Zhai, M.Z., 1990. Geochemistry of Hannuoba basalts, eastern China: constraints on the origin of continental alkalic and tholeiitic basalt. Chem. Geol. 88, 1–33.
Zhou, X.H., Armstrong, R.L., 1982. Cenozoic volcanic rocks of eastern China-secular and geographic trends in chemistry and strontium isotopic composition. Earth Planet. Sci. Lett. 58, 301–329.
Zindler, A., Hart, S.R., 1986. Chemical geodynamics. Annu. Rev. Earth Planet. Sci. 14, 493–571.
Zou, H., Zindler, A., Xu, X., Qi, Q., 2000. Major, trace element, and Nd, Sr and Pb isotope studies of Cenozoic basalts in SE China: mantle sources, regional variations, and tectonic significance. Chem. Geol. 171, 33–47.
Zou, H., Reid, M.R., Liu, Y., Yao, Y., Xu, X., Fan, Q., 2003. Constraints on the origin of historic potassic basalts from northeast China by U–Th disequilibrium data. Chem. Geol. 200, 189–201.